VYSOKÉ UČENÍ TECHNICKÉ V BRNĚ
BRNO UNIVERSITY OF TECHNOLOGY

FAKULTA STAVEBNÍ
FACULTY OF CIVIL ENGINEERING

ÚSTAV GEOTECHNIKY
INSTITUTE OF GEOTECHNICS

DESIGN OF DIAPHRAGM WALL AFFECTED BY EXCAVATION FROM BOTH SIDES
NÁVRH PODZEMNÍ STĚNY OVLIVNĚNÉ VÝKOPEM Z OBOU STRAN

DIPLOMOVÁ PRÁCE
DIPLOMA THESIS

AUTOR PRÁCE
AUTHOR
Bc. Veronika Kočičková

VEDOUCÍ PRÁCE
SUPERVISOR
MICHAL UHRIN

BRNO 2017

VYSOKÉ UČENÍ TECHNICKÉ V BRNĚ
FAKULTA STAVEBNÍ

Studijní program	N3607 Stavební inženýrství
Typ studijního programu	Navazující magisterský studijní program s prezenční formou studia
Studijní obor	3607T009 Konstrukce a dopravní stavby
Pracoviště	Ústav geotechniky

ZADÁNÍ DIPLOMOVÉ PRÁCE

Student	Bc. Veronika Kočičková
Název	Design of Diaphragm Wall Affected by Excavation from Both Sides
Vedoucí práce	Michal Uhrin
Datum zadání	31. 3. 2016
Datum odevzdání	13. 1. 2017

V Brně dne 31. 3. 2016

doc. Ing. Lumír Miča, Ph.D. Vedoucí ústavu	prof. Ing. Rostislav Drochytka, CSc., MBA Děkan Fakulty stavební VUT

PODKLADY A LITERATURA

1) Ground conditions - Report. Drawings. Design parameters.
2) Geometrical arrangement - Drawings.
3) Design criteria - Reports.
4) Miscellaneous - Presentations, technical papers, photos.

ZÁSADY PRO VYPRACOVÁNÍ

Subject:
Structural/geotechnical engineering analysis and design of diaphragm wall for TBM launch shaft adjacent to metro station. Due to the station interface, one side of the launch shaft will be affected by excavation from both sides. And by subsequent backfill.
Tasks:
- Desk study of inputs and design criteria.
- Internet research of calculation methods (see below).
- Analytical models and calculations.
- Structural design checks.
- Summary of inputs, methodology and outputs / findings / conclusions into formal report.

Items to be addressed:
- General description of the structure;
- Description of construction sequence;
- Description of ground and groundwater conditions;
- Research regarding temperature load on steel struts;
- Analytical models: 1 characteristic section. 2 methodologies - subgrade reaction (as far as software capability allows) and geotechnical FEM. Comparison of results. Additionally, structural FEM model of 1 lateral support frame.
- Structural design checks: Diaphragm wall in analysed section. 1 lateral support frame (struts and waler beams).

Specifications:
- Geotechnical analyses to consider excavation from both sides (station interface) and backfill inside.
- Lateral support frame check against disproportionate collapse (accidental loss of any single strut).
- Diaphragm wall shared with station being permanent structure.
- TBM loads excluded from consideration.
- Standards: Eurocodes or as per Design Criteria.

Deliverable:
- Report in English language.

STRUKTURA DIPLOMOVÉ PRÁCE

VŠKP vypracujte a rozčleňte podle dále uvedené struktury:
1. Textová část VŠKP zpracovaná podle Směrnice rektora "Úprava, odevzdávání, zveřejňování a uchovávání vysokoškolských kvalifikačních prací" a Směrnice děkana "Úprava, odevzdávání, zveřejňování a uchovávání vysokoškolských kvalifikačních prací na FAST VUT" (povinná součást VŠKP).
2. Přílohy textové části VŠKP zpracované podle Směrnice rektora "Úprava, odevzdávání, zveřejňování a uchovávání vysokoškolských kvalifikačních prací" a Směrnice děkana "Úprava, odevzdávání, zveřejňování a uchovávání vysokoškolských kvalifikačních prací na FAST VUT" (nepovinná součást VŠKP v případě, že přílohy nejsou součástí textové části VŠKP, ale textovou část doplňují).

Michal Uhrin
Vedoucí diplomové práce

ABSTRAKT

Cílem této diplomové práce byl zjednodušený návrh podzemní stěny ovlivněné výkopem z obou stran. Tato stěna je součástí dočasné šachty pro výměnu tunelovacích strojů a zároveň je trvalou konstrukcí přilehlé stanice metra. Součástí práce je popis postupu výstavby podzemních stěn, hloubení šachty, hloubení přilehlé stanice metra a následné vytvoření tunelových rour pro metro a zasypání šachty. Nedílnou součástí práce je pojednání o geologických podmínkách a zhodnocení geotechnických parametrů. Dále byla vypracována rešerše na téma teplotního namáhání rozpěr a výsledky této rešerše byly aplikovány na návrh rozpěr. Pro splnění požadavků zadání bylo vytvořeno několik modelů konstrukce šachty a přilehlé stanice metra v programu Plaxis a jeden model podzemní stěny šachty v programu Geo5. Výstupy z těchto modelů byly následně mezi sebou porovnány. Dále byl vytvořen model rozpěrného rámu v programu Scia Engineer. Výstupy z programů Plaxis a Scia Engineer byly použity jako podklad pro posouzení konstrukce. Toto posouzení bylo provedeno dle Eurokódů. Podzemní stěna i rozpěrný rám byly navrženy tak, aby přenesly účinky od zatížení, která byla uvažována v této práci. Pro zjednodušení byla zanedbána proměnná zatížení od pracovních strojů a jako jediné proměnné zatížení bylo uvažováno teplotní zatížení rozpěr. Rozpěrný rám byl také navržen na mimořádné zatížení – ztrátu rozpěry.

KLÍČOVÁ SLOVA

podzemní stěna, namáhání teplotou, rozpěrný rám

ABSTRACT

The aim of this thesis was simplified design of diaphragm wall affected by excavation from both sides. This wall is a part of temporary shaft that serves for exchange of tunnel boring machines and at the same time it is a permanent structure of an adjacent metro station. Part of the thesis deals with description of construction sequence of diaphragm walls, excavation of the shaft, excavation of the adjacent metro station and following construction of metro tubes and backfilling of the shaft. Inseparable part of the thesis is assessment of geological conditions and geotechnical parameters. Furthermore, a study on temperature loads on struts was carried out and the results of the study were used for design of the struts. To fulfil the requirements of the assignment several models of the shaft structure and adjacent metro station were built in program Plaxis and one model of the diaphragm wall of the shaft was created in program Geo5. The model outputs were subsequently compared to each other. Furthermore a model of lateral support frame was created in program Scia Engineer. Outputs from programs Plaxis and Scia Engineer were used as a basis for design checks of the structure. The design checks were done according to Eurocodes. The diaphragm wall and the lateral support frame were designed to support the loads considered in this thesis. In order to simplify the calculation variable loads from construction machines were not considered and the only variable load considered was the temperature load on struts. Lateral support frame was also designed to accidental load – loss of a strut.

KEY WORDS

diaphragm wall, temperature loads, lateral support frame

BIBLIOGRAFICKÁ CITACE VŠKP

Bc. Veronika Kočičková *Design of Diaphragm Wall Affected by Excavation from Both Sides.* Brno, 2016. 75 s., 14 s. příl. Diplomová práce. Vysoké učení technické v Brně, Fakulta stavební, Ústav geotechniky. Vedoucí práce Michal Uhrin

PROHLÁŠENÍ

Prohlašuji, že jsem diplomovou práci zpracovala samostatně a že jsem uvedla všechny použité informační zdroje.

V Brně dne 10. 01. 2017

Bc. Veronika Kočičková
autor práce

PODĚKOVÁNÍ

Na tomto místě bych chtěla poděkovat panu Ing. Michalovi Uhrinovi za odborné vedení práce, cenné rady a připomínky, ochotu a vstřícný přístup v průběhu zpracování této diplomové práce. Dále bych chtěla poděkovat pracovníkům ústavu geotechniky za vstřícný přístup během celého studia.

List of contents

Introduction

The thesis deals with simplified design within a virtual project of a shaft where one diaphragm wall is affected by excavation from both sides. This diaphragm wall will act as permanent structure. In the first Chapter there is general information and description of the structure given but also there is description of construction sequence of the shaft and adjacent metro station. Assessment of geological and geotechnical conditions is also part of the thesis and it is provided in Chapter two. Furthermore, the assignment of the thesis requires research on thermal loads acting on struts. This research is summarised in Chapter three and then one of the conclusions of the research is used in design check of a strut in Chapter four. One of the main objectives of the thesis was to create several calculation models and compare their results. There were created three models in geotechnical FEM software Plaxis with two different material models and with different settings for Clay layer that is decisive for this structure. There is also a subgrade reaction model in Geo5. However this model could not represent all construction phases and therefore the comparison with FEM Plaxis model is limited only to the phase of construction, where the base slab of the shaft is created. Another main part of the thesis was design of the diaphragm wall and design of a lateral support frame. All design checks were done according to Eurocodes. The lateral support frame was also checked against disproportionate collapse (accidental loss of the most loaded strut – in this case it was the longer corner strut).

1 PROJECT DESCRIPTION

1.1 Basic information

There is a new metro line planned in the area of interest. The line is divided into two separate tunnels – eastbound and westbound. Both tunnels are driven by full face earth pressure balance shields tunnel boring machines (EPB TBMs), but there is a necessity to change these machines for slurry shields (SPB TBMs) at a given location in order to continue tunnelling of the line.

For this purpose a shaft is planned in a place of the exchange. There is only a limited space for the shaft on the surface and the Client has only certain means for excavation (technical and financial). Therefore the shaft is designed so that it has a common wall with a planned metro station.

There are requirements on the dimensions of the shaft at the side of the operator of TBMs because it is necessary to dismantle the incoming machines inside of the shaft and then it is necessary to assemble the new machines partially on the surface and then lower them down and finish the assembly inside of the shaft. The general requirements are:

- The minimum clearance under the lower level of the struts to be 4 m from the tunnel central line.
- The minimum lateral distance between the shield and the diaphragm wall to be 2 m.
- The minimum dimensions of the assembly opening to be 8x6 m.
- The heaviest part of the shield capable of vertical handling to be 120 tonnes.

[1]

1.2 Design basis

The design of the structural elements is based on Eurocodes. Eurocode 0 is used for the basis of structural design, Eurocode 1 is used for the actions on structures, Eurocode 2 is used for the design of reinforced concrete diaphragm wall, Eurocode 3 is used for the design of lateral support frame and Eurocode 7 (design approach 2) is used for geotechnical part of the design.

1.3 Structure description

For sketches see Appendix 1, Appendix 2 and Appendix 3.

Reinforced concrete diaphragm walls were chosen as a construction method that fits the requirements of the Client and is suitable considering the geotechnical conditions. The shaft will be braced in four levels by steel frames (welded sections are used for waler beams, tubes 1020/25 are used for braces). The bottom of the shaft is designed as 1.5 m thick reinforced concrete slab. Concrete grade C35/45, steel B500B for concrete reinforcement and steel of the grade S235 and S355 for strutting system will be used. The dimensions of the shaft are given by the above mentioned requirements and limitations:

- footprint: 22.05 m x 27.6 m
- depth of the shaft up to the formation level of the bottom slab:
  31.5 m below the ground surface
- thickness of the diaphragm walls: 1.5 m
- length of the D-walls: 41.0 m
- maximum width of panels: 6.7 m

The shaft is made of four walls from which three walls are temporary and one wall is permanent. The permanent wall is the wall that is adjacent to metro station and that is affected by excavation from both sides. For the purposes of this thesis this wall is only designed for ultimate limit state (precisely only to bending moments' envelope because the bending moments are significant on this structure) but normally it would be necessary to design it also to serviceability limit state and check for the width of cracks.

The first 3.0 m of the excavation are in made ground but the structure is situated mostly in a clay environment; bigger part of the structure is under the ground water level (groundwater table level is 13.8 m below the ground surface). [1]

1.4 Phases of construction

For sketches see Appendix 4 and Appendix 5.

Phase 1: Preparation of working platform

At first a pile wall on one side of the excavation will be constructed (there are existing buildings on this side). The distance of the wall from the planned diaphragm wall is 2.0 m. The pile wall is designed as contiguous. The diameter of the piles is 0.8 m, the length of the piles is 10.0 m. Then the heads of the piles will be cut and capping beam will be made. The piles are anchored in the upper third of their depths. Other sides of the excavation are designed in slope at 1:1 crossfall.
The excavation is up to -2.0 m under the surface.

Phase 2: Construction of diaphragm walls

In order to keep the precise alignment and continuity of the diaphragm walls it is necessary to construct the guiding walls. These walls are constructed in trench so that the inner clearance corresponds to the width of diaphragm walls + 50 mm. The inner side of the diaphragm wall is in alignment with the face of the guiding wall whereas the outer side of the diaphragm wall has allowance of 50 mm. The guiding walls are designed as L-shaped with the depth of 1.5 m and thickness of 0.2 m. They are made of lightly reinforced concrete and they are braced. This temporary support also helps to keep grabs in a vertical position and it reduces possible negative effects of bentonite slurry level fluctuation.

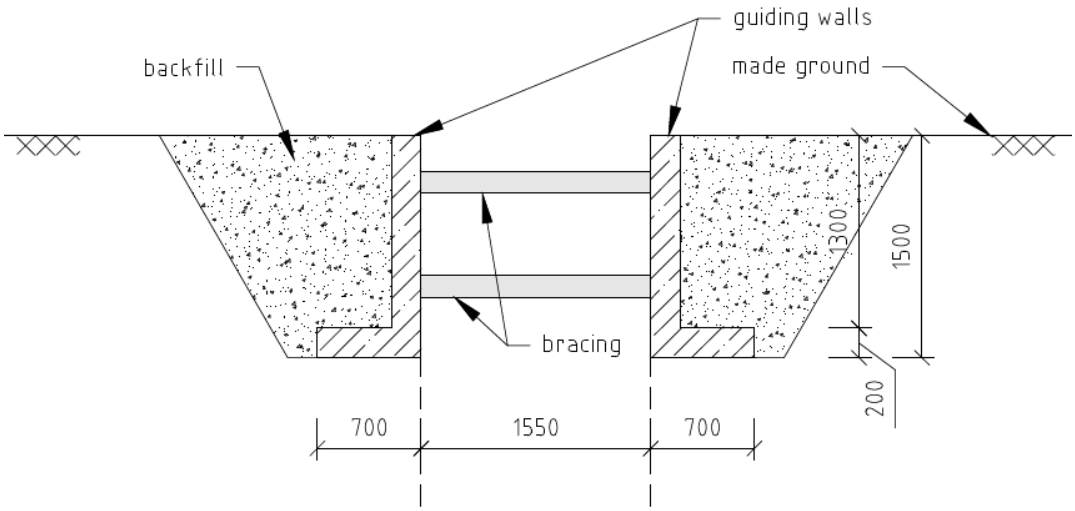

Figure 1.1 Scheme of guiding walls

The construction of D-walls starts with the starting panels. The trench is made to the whole depth by grabs (these can be mechanical or hydraulic – considering the depth of the D-walls it is more suitable to use the hydraulic ones) or by hydraulic cutter. In order to obtain bigger width of the panel, it is excavated in three steps. At first the right or left side of the panel is excavated, then the other side and at the end the middle part is excavated. Also the corner panels and T-shaped panels are excavated in multiple steps.

Before we start the trench excavation the bentonite slurry plant has to be prepared. The slurry is used to balance the soil pressure to keep the wall excavation from collapse. The mixture has to be cleaned during the construction in order to keep its properties (density, pH, viscosity). The mixture is recycled in the plant where it is separated from soil debris and then it is pumped back to the excavation.

When the trench is done the stop-ends are placed. In this case it is necessary to obtain water tight walls. Therefore the steel groove stop-ends with water stops are going to be used.

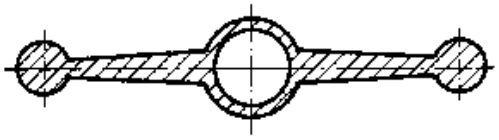

Figure 1.2 Water stop shape [2]

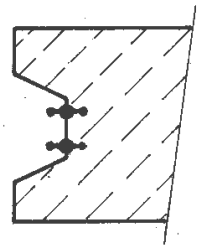

Figure 1.3 Joint between two panels [2]

When the bottom of the trench is reached and bentonite cleaned the reinforcement cage can be lowered to its final position. The cage is made of vertical bars and horizontal bars and sufficient bracing bars so that it is rigid enough to be lowered and lifted while placing into position and it is designed to the structural loads. The cage is suspended from guiding

walls and it has to be kept vertical. There has to be enough space left for two or three tremie pipes inside of the reinforcement cage.

Concreting of the panels is done bottom–up. While concreting the tremies are continuously lifted up but they should always stay immersed in the fresh concrete for at least 0.5 m to avoid slurry pockets. In order to obtain clear concrete throughout the wall it should be overpoured at the top.

When the starting panel concrete sets, the excavation of trench for following panel is done. Further it is necessary to take out the stop-ends (while the water stop stays in place). This is done, for example, with the help of pounder that is locked into the stop end and moves downwards. Then the secondary panel trench is reinforced and filled with concrete.
[2] [3] [4] [5]

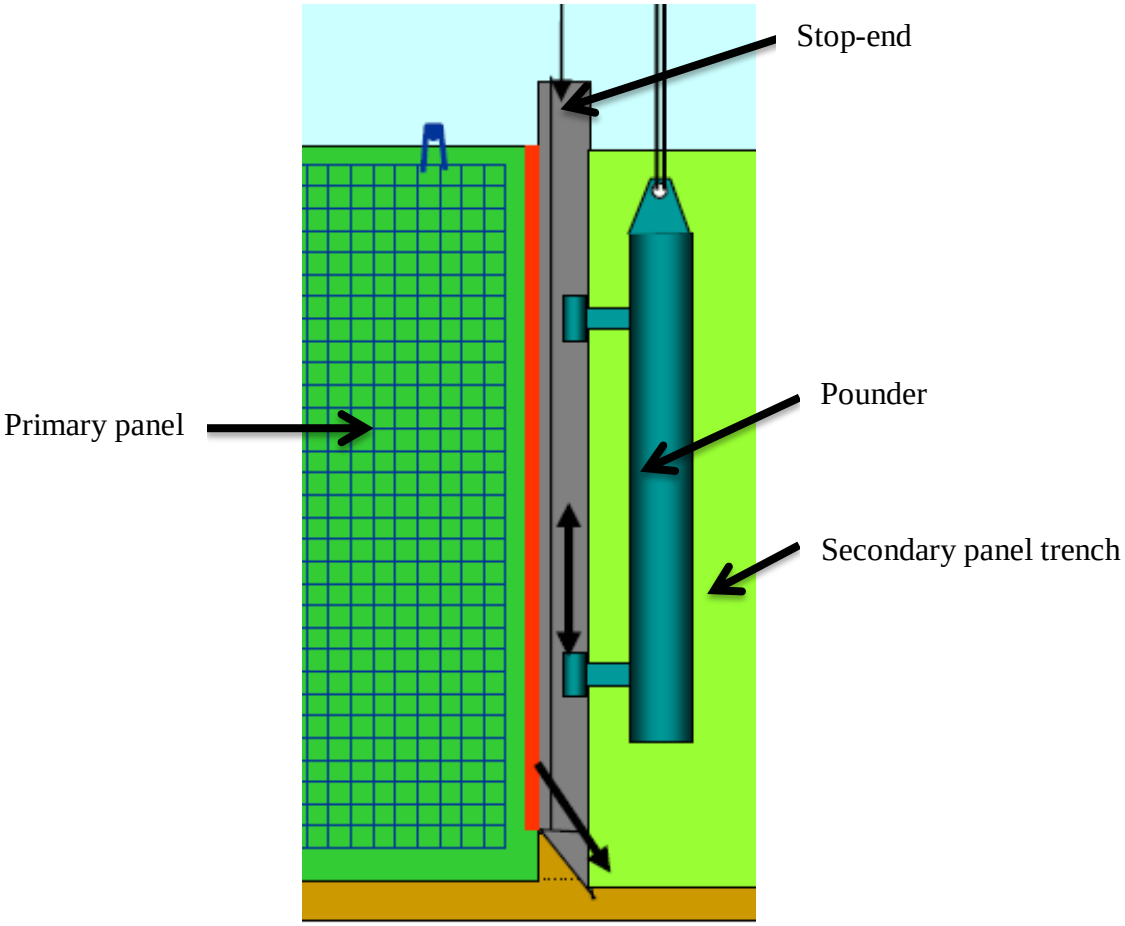

Figure 1.4 Removing of stop-ends

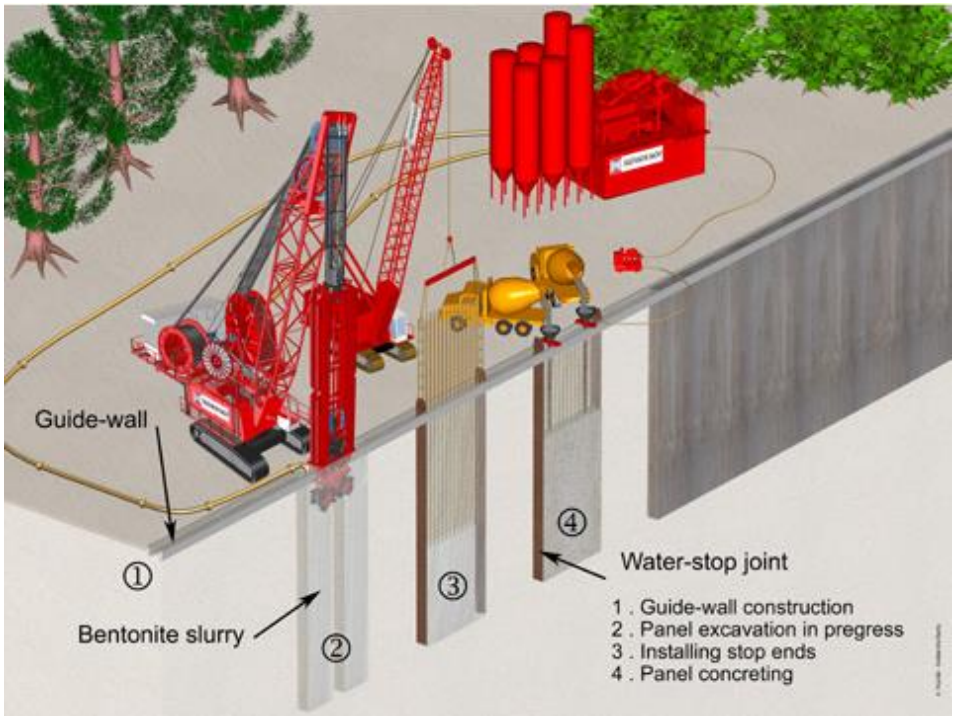

Figure 1.5 Construction of diaphragm walls [3]

When all shaft panels are set the heads of the panels will be cut by 0.5 m and capping beam will be constructed.

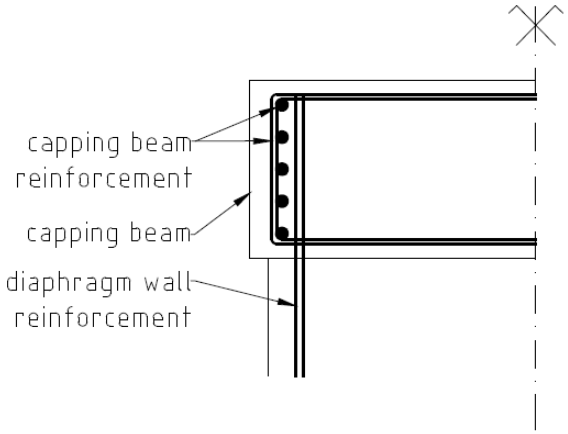

Figure 1.6 Scheme of capping beam reinforcement

Then the excavation at the work platform will continue to the depth of 3.5 m below the ground surface.

Phase 3: Excavation of the inside of the shaft

Furthermore the excavation will only continue on the inside of the shaft. First level of excavation is -4.8 m under the surface, first bracing level is -4.05 m under the surface.

Second level of excavation is -10.95 m and second bracing level is -10.2 m. To continue the excavation dewatering has to be established. Third level of excavation (-16.7 m) and bracing (-15.95 m) is under the groundwater level. Fourth level of excavation is -21.6 m and fourth level of bracing is -20.85 m. Then the excavation will be done up to the formation level of the base slab (-31.5 m) and a temporary base slab will be constructed.

Phase 4: Excavation of the metro station

The other side of one of the diaphragm walls will be excavated as a part of construction of the adjacent metro station. The excavation is done in multiple steps according to the levels of metro station ceilings that will act as permanent bracing system. First level of excavation is –10.2 m, second level –15.95 m, third level –21.45 m. Formation level of metro station base slab is -30.75 m.

Phase 5: Metro tubes and backfill of the shaft

After the TBMs are changed and the new TBMs leave the shaft, a ceiling slab for metro tube is going to be constructed. Then the shaft will be filled by backfilling material and bracing frames will be removed.

2 GEOTECHNICAL CONDITIONS

2.1 Geological model

The shaft is situated in a simple geological profile. The upper layer (thickness of approximately 3 m) is composed of made ground. Then there is a layer of Neogene clays up to the depth of 38 m. These clays are considered to be stiff to very hard, slightly overconsolidated to overconsolidated. Under this layer there is a heavily weather limestone. Its quality and properties increase with depth. The level of the underground water was located at the depth of 13.8 m below the ground surface. Although the nature of it is questionable given it is located in Clay stratum.

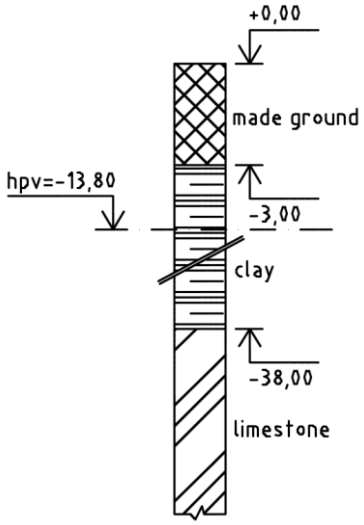

Figure 2.1 Geological model

2.2 Geotechnical parameters

Geotechnical parameters were determined on the basis of engineering geological survey. This survey was carried out insufficiently – there were no parameters for the upper layer of geological profile (made ground) and also the layer of limestone was not very well described.

On the other hand there were many tests conducted on the layer of clays that is determinative layer for this shaft. Regarding the field tests, the total of 5 pressuremeter tests, 8 standard penetration tests and 9 cored boreholes for taking disturbed and undisturbed samples were carried out in the area of the future shaft and its close vicinity up

to 35 m. However the sampling method locally available (by the use of simple tube core barrel) leads to significant disturbance and affects the reliability of some test results. Samples disturbance is particularly highlighted on oedometer tests results, as well as water content and unit weight determination.

Laboratory measurements comprised the total of 7 triaxial tests and 15 oedometer tests. Despite the number of the tests, the quality of the results was at a low level. For example there was no correlation between the measured values of individual tests and no comments were added to the results of EGS. Furthermore the oedometer test results and the pressuremeter tests results could lead to consider that clays are underconsolidated to normally consolidated, whereas the visual description of the clay unit, confirmed by high SPT values and shear strength parameters (triaxial tests), indicate slightly overconsosolidated to overconsolidated clays.

Figure 2.2 Samples from field test (DBH)

Figure 2.3 Field test (SPT)

The properties of made ground were determined based on engineering judgement considering experience with local conditions. Properties of limestone were based on the pressuremeter tests and photo documentation. Regarding the layer of clay, the geotechnical parameters were determined from the results of laboratory tests (triaxial tests and oedometer tests for the determination of strength-related and deformational properties of clay) and field tests (the results of pressuremeter tests provided the basis for the determination of the undrained shear strength-depth curve; the value of earth pressure at rest K_0 and the undrained modulus of deformation were determined from the results of pressuremeter tests) and by correlation between field and laboratory tests. [1] [6]

In the table 2.1 below you can see the established geotechnical parameters for each soil or rock layer. It is necessary to keep in mind that the geotechnical parameters were not established ideally and therefore there are reservations in its values. The estimated values are on conservative side (for example low modulus of elasticity for Clay).

Table 2.1 Geotechnical parameters (refer to List of shortcuts at the end of the thesis)

	γ [kN/m^3]	φ_{cv} [°]	φ' [°]	c' [kPa]	S_u [kPa]	C_c	C_s	K_0	ν	E' [MPa]
Made ground	20	-	20	10	-	-	-	0.5	0.3	10
Clay	20	26	21	60	60-150	0.11	0.015	1.0	0.3	35
Limestone	21	-	35	150	-	-	-	0.5	0.25	300

3 THERMAL LOADS ON STRUTS

The main load acting on struts is load created by ground and water pressure. Furthermore there are indirect loads as for example from temperature.

Thermal load can be caused by changes of surface temperature of the struts. The temperature change can be caused by differences in temperature of ambient air during the day and during the year but it can also be caused by sun-shining. In case when the strut is situated on a direct sunshine, its upper surface is getting warm faster than the lower surface and the strut is loaded by differential thermal stress (stress changes about to the vertical axis). Another example could be a strut that is partially situated in a shadow and partially in the sun. Then the change in thermal stress would not only be in vertical axis but also in horizontal axis. Thermal load can cause additional axial normal forces but also additional bending moments. For the purposes of this thesis only even stress from temperature is considered.

3.1 Calculation of thermal loads

3.1.1 Calculation based only on linear elasticity

In this approach an increase/decrease in temperature is independent of the length of the strut itself. This comes from the definition of strain – it is defined as a proportion (there are no units or dimensions). Strain (ε) is defined as a ration between the change of length (ΔL) and the original length (L).

$$\varepsilon = \frac{\Delta L}{L}$$

Strain is also used to define the Young's modulus (E):

$$\mathrm{E} = \frac{\sigma}{\varepsilon}$$

where (σ) stands for stress.

It also occurs in the definition of the thermal coefficient of expansion (α) as induced strain per degree change in temperature (ΔT).

$$\alpha = \frac{\varepsilon}{\Delta T}$$

Then by rearranging the above equations we get an equation from which we can derive force (F) from temperature change.

$$E = \frac{\sigma}{\alpha * \Delta T}$$

(rewrite with σ = F/A where (A) represents cross sectional area)

$$E = \frac{F}{A * \alpha * \Delta T}$$

By rearrange of this equation we get $F = E * A * \alpha * \Delta T$

We can see from the equation above that the force from load change is independent on the length of the strut. On the other hand we can also see that a strut with bigger cross-sectional area will potentially induce a greater thermal load. Therefore using more steel to resist thermal loads actually generates even more thermal load.

In this force equation it is assumed that the strut is fully restrained at its ends against movement due to expansion.

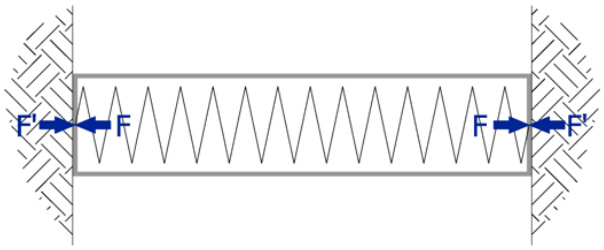

Figure 3.1 Strut in equilibrium at installation temperature [7]

There is a certain amount of load in the strut from pre-stress and lateral earth pressures etc. If the temperature in the strut increases, it would need to expand, generating resisting forces from the surrounding ground.

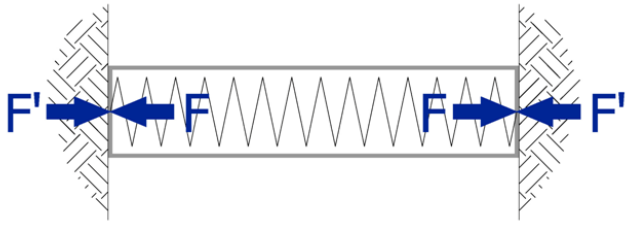

Figure 3.2 Strut fully restrained by a rigid support structure [7]

In Figure 3.2 we can see that all of the potential expansion from temperature effects is translated into extra axial load.

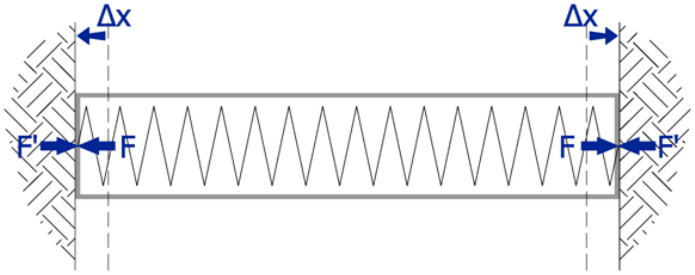

Figure 3.3 Strut partially restrained by semi-flexible support structure [7]

In Figure 3.3 we can see a solution where the strut is allowed to expand to a certain degree. In this case, the load induced by temperature in the strut is reduced.

3.1.2 Calculation according to Chapman et al (1972)

In this approach the load changes in struts due to temperature changes can be estimated if the modulus of deformation of the cut wall can be estimated. The force equation is based on combination of relations for elastic displacement of the cut wall with the effect of temperature on load and displacement of a strut. [8]

$$F = \frac{A * E_s * \alpha * \Delta T}{1 + \frac{3 * n * A * E_s * H}{A_w * E_{soil} * L}}$$

where (F) is the load change due to temperature, (E_s) is the modulus of steel, (α) is the thermal coefficient of expansion (1.2e-05 for steel), (ΔT) is the change in temperature, $(n * A)$ is the area of struts acting against the area of the cut wall (A_w), (H) is the height of excavation, (E_{soil}) is the Young's modulus of soil, (L) is the length of the strut.

The assumption for this equation is that the struts are not fully restrained. However the load change will approach the load changes for restrained struts if the soil modulus is high, if the total area of steel struts divided by the area of the cut wall is low, if the length of the strut is great with respect to the height of the excavation. [8]

3.1.3 Conclusions

Both ways of calculation are based on linear elasticity, nevertheless the equation by Chapman et al takes in account the length of the struts and the height of excavation and it is assumed that the strut is not fully restrained.

Temperature changes can cause significant changes in strut loads and therefore it should be considered in the design of braced excavations. However the load changes due to high increase/decrease in temperature should be considered only if the earth pressures are based on data obtained for relatively constant temperature or small changes in temperature. [8]

The load change due to temperature should be considered as extra axial load but also when acting on an eccentricity it creates bending moments in struts.

4 STRUCTURAL DESIGN

In this thesis the structural design is focused on the diaphragm wall that is affected by excavation from both sides and on lateral support frame situated in the lowest level of bracing system (it is the most loaded frame). In order to assess the loads on different structural elements more types of software and models where used.

Table 4.1Models used in the thesis

Model	Type of analysis	Structural element
Plaxis - Modified Cam Clay (undrained) - Mohr-Coulomb (undrained) - Mohr-Coulomb (drained)	 FEM FEM FEM	Structure
Geo5 - effective parameters	 bedding reaction model	Structure
SCIA	FEM	Bracing frame

4.1 Plaxis

Plaxis is software based on finite element method. Constitutive material models are used for the simulation of non-linear and time-dependent behaviour of soils. In this thesis there were used two different constitutive models for clay.

4.1.1 Modified Cam Clay model (undrained)

The Modified Cam Clay (hereinafter referred to as CC) material model is used for clay with undrained conditions. For the layer of Made ground and Limestone the Mohr-Coulomb (hereinafter referred to as MC) material model with drained conditions is used.

The advantages of CC model are:

- different values of soil stiffness for loading and unloading
- stiffness value is dependent on pressure
- capability of predicting the increase in undrained shear strength with depth in the case of the undrained analysis

Undrained (or short-term) conditions are in Plaxis simulated by material behaviour in which stiffness and strength are defined in terms of effective properties. Large bulk stiffness for water is automatically applied to make soil incompressible and excess pore pressures are calculated, even above the phreatic level.

Drained (or long-term) conditions stand for material behaviour in which stiffness and strength are defined in effective properties.

The model is designed as a Plane-strain model with 15-noded elements. Its dimensions are 400 m of width x 200 m of depth. The shaft is situated axially because of the symmetry control of the first part of calculation.

The soil parameters are stated in Table 2.1. The interface parameter R_{inter} was set to 0.5 for Made ground and Limestone. For CC model it was necessary to put in the stiffness parameters (λ, κ, ν'_{ur} and e_{init}) and interface material properties (c'_{ref}, φ'). These parameters were taken from the geotechnical interpretative report where they were established by correlation of the data from the geotechnical survey.

Table 4.2 Parameters for CC model

Soil parameters	λ [-]	κ [-]	ν'_{ur} [-]	e_{init} [-]
	0.056	8e-3	0.15	0.8
Interface parameters	c'_{ref} [kN/m^2]	φ'[°]		
	1	15		

All structural elements were modelled as plates for which the elastic material model is used. Plates that are on contact with soil are modelled with interfaces.

The modulus of elasticity for concrete was according to Eurocode considered to be E = 33.5 GPa, for steel struts E = 210 GPa.

Table 4.3 Plates parameters

	EA [kN/m]	EI [kNm^2/m]	d [m]	w [kN/m/m]
diaphragm walls	50.25e6	9.42e6	1.5	-*
base slab (shaft)	50.25e6	9.42e6	1.5	-
ceilings MS	40.20e6	4.82e6	1.2	30
base slab MS	67.00e6	22.33e6	2.0	-
strut	5.471e6	676.2e3	-	2.041**

* the weight of the D-wall was neglected because soil is changed for concrete of approximately same weight and because in the model the D-wall is modelled by plate and the original soil stays in place

** the weight of struts was calculated as average cross sectional area of struts per meter times the unit weight of steel:

$$w = A_{strut} * \gamma_{steel} = 0.026 * 78.5 = 2.041 \text{ kN/m/m.}$$

All plates of the shaft are modelled as axial compared to the real dimensions. The adjacent metro station is modelled as shortened – the station is actually much longer than in the model but considering the supposed static behaviour of MS ceilings it can be neglected.

The steel struts in the shaft are connected to the diaphragm walls by hinges, on the contrary the reinforced concrete MS ceilings are considered to be fully fixed in the diaphragm walls. The base slab of the shaft and the base slab of MS are also considered to be fully fixed to the diaphragm walls.

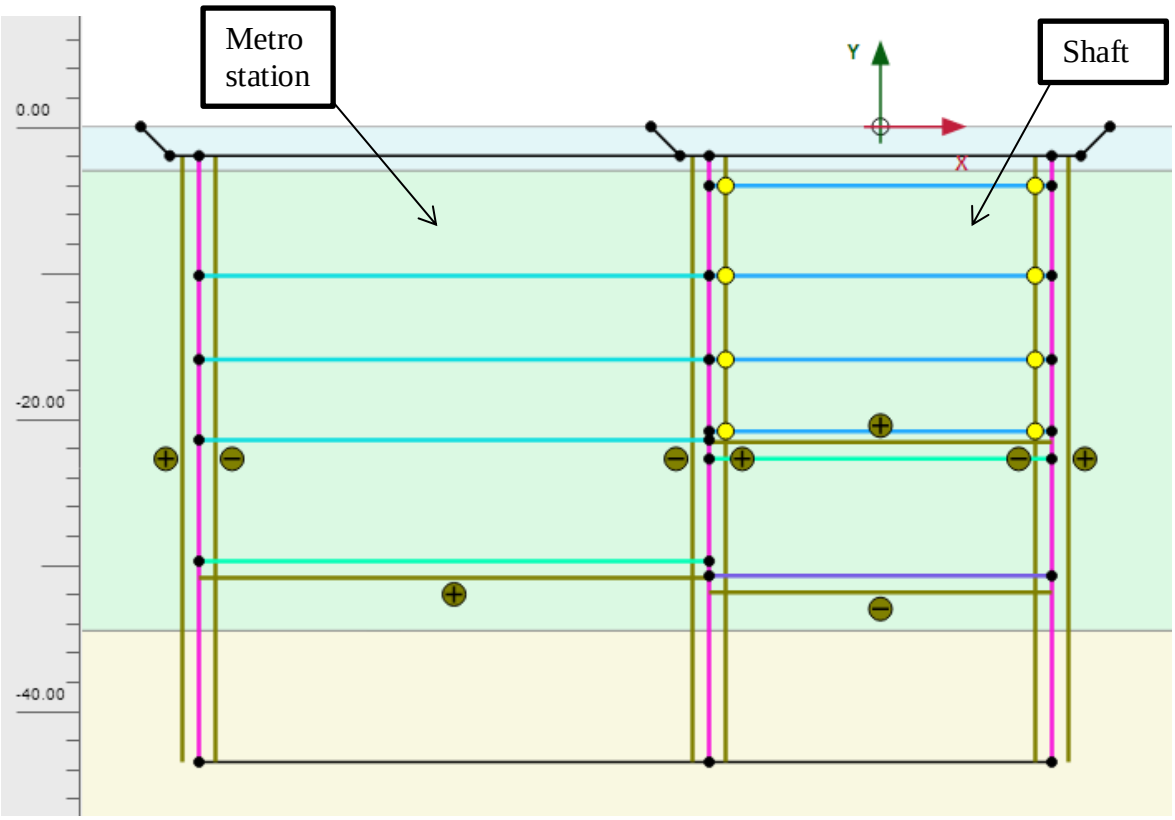

Figure 4.1 Structure model

Soils and interfaces	Plates
Backfill	base slab
clay	base slab MS
limestone	ceiling MS
made ground	D-wall
	strut

Figure 4.2 Legend of materials

The finite elements mesh is refined in the inside of the structures and in a certain distance from the structure to the coarseness factor 0.25, otherwise the coarseness factor is 0.8. The total number of elements is 2 928.

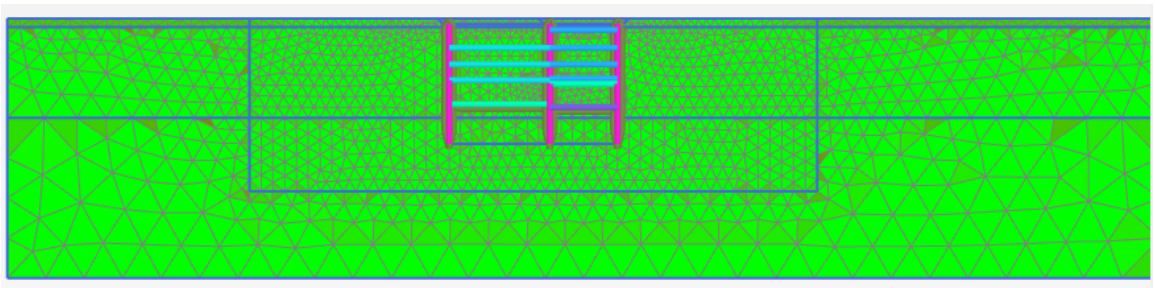

Figure 4.3 Finite element mesh

The dewatering of the inside of the structures was taken in consideration by setting local groundwater levels in clusters inside of the structure and in a close proximity underneath it. The groundwater levels were set according to the phases of construction. Clusters from which the soil was excavated during the phases of construction are set as dry.

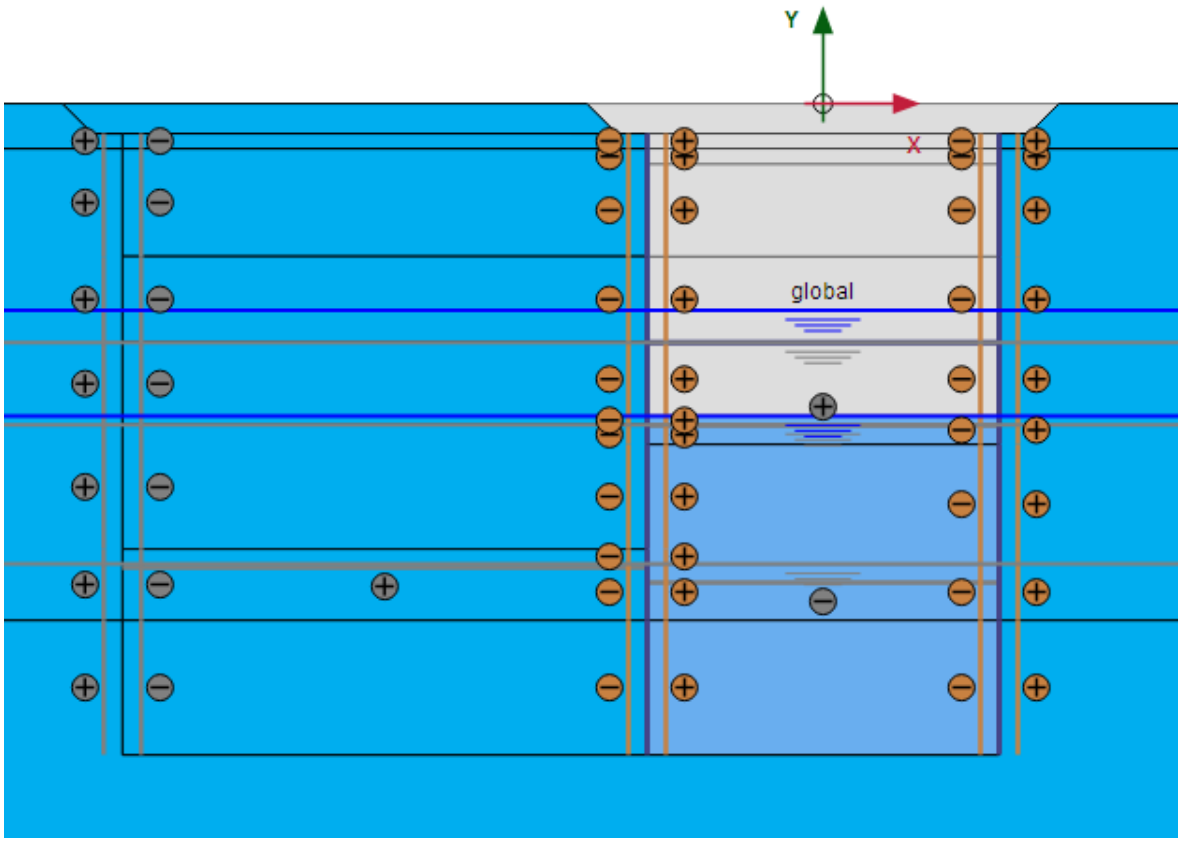

Figure 4.4 Groundwater conditions – you can see two water levels in the picture. The upper level is the phreatic groundwater level, the lower level is customised groundwater level inside of the structure due to dewatering.

<u>Phases of construction set in the model:</u>

Phase 0: K_0 procedure

Phase 1: primary excavation (inside of the shaft), activation of diaphragm walls

Phase 2: excavation to the 1st bracing level

Phase 3: activation of the 1st bracing level, excavation to the 2nd bracing level

Phase 4: activation of the 2nd bracing level, excavation to the 3rd bracing level

Phase 5: activation of the 3rd bracing level, excavation to the 4th bracing level

Phase 6: activation of the 4th bracing level, excavation to the level of base slab

Phase 7: activation of the base slab

Phase 8: primary excavation (inside of metro station), activation of diaphragm wall

Phase 9: excavation to the 1st MS ceiling level

Phase 10: activation of the 1st MS ceiling level, excavation to the 2nd MS ceiling level

Phase 11: activation of the 2nd MS ceiling level, excavation to the 3rd MS ceiling level

Phase 12: activation of the 3rd MS ceiling level, excavation to the level of MS base slab

Phase 13: activation of MS base slab

Phase 14: activation of ceiling slab for metro tube inside of the shaft

Phase 15: backfilling to the 4th bracing level, deactivation of the 4th bracing level

Phase 16: backfilling to the 3rd bracing level, deactivation of the 3rd bracing level

Phase 17: backfilling to the 2nd bracing level, deactivation of the 2nd bracing level

Phase 18: backfilling to the 1st bracing level, deactivation of the 1st bracing level

Phase 19: backfilling of the upper part of the shaft

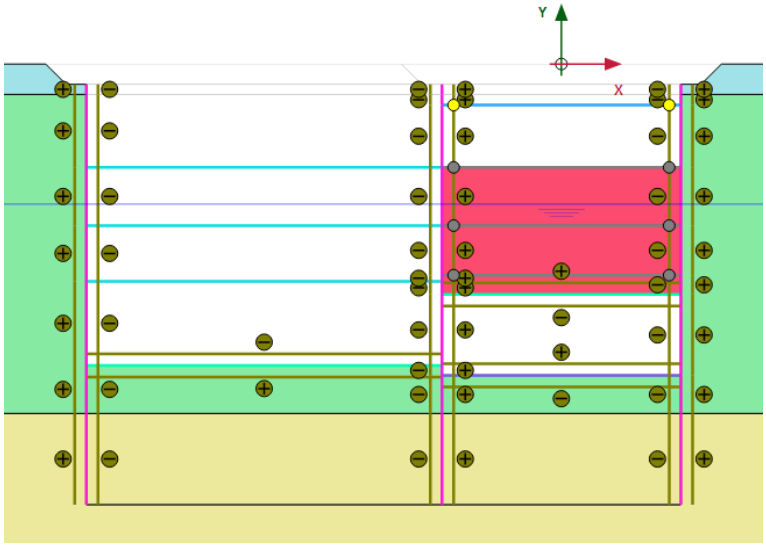

Figure 4.5 Phase 17

Backfilling material:

There are different possibilities for the backfilling material of the shaft. Preferably it should be a non-porous material. In this thesis the materials used for backfilling were: soil improved with cement, polystyrene concrete and made ground. In this thesis it is assumed that the soil improved with cement is non-porous. In case of made ground it would be necessary to establish permanent dewatering of the inside of the shaft so that the water could not accumulate and excess water pressure would not be created.

The purpose of trying different materials was to find out if it would be possible to reduce the final vertical displacement of the backfill.

Table 4.4 Backfilling materials

	γ [kN/m^3]	E [MPa]	ν [-]	c_{ref} [kN/m^2]	φ [°]	setting
Soil with cement	18	75	0.3	15	40	MC non-porous
Polystyrene concrete	9	56	0.2	-	-	LE non-porous
Made ground	20	10	0.3	10	20	MC drained

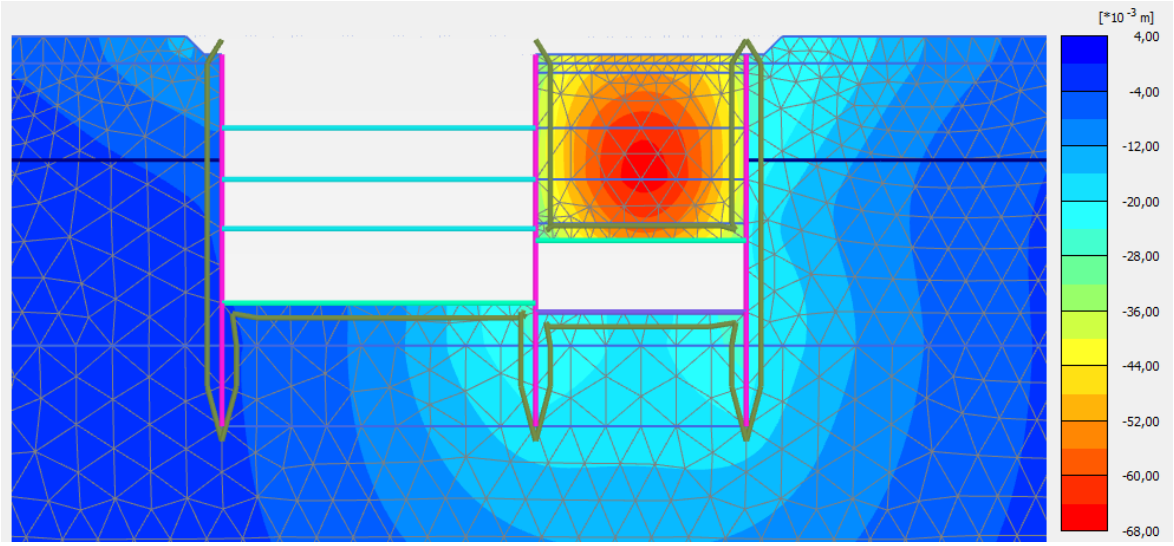

Figure 4.6 Soil displacements u_y for soil with cement as backfilling material

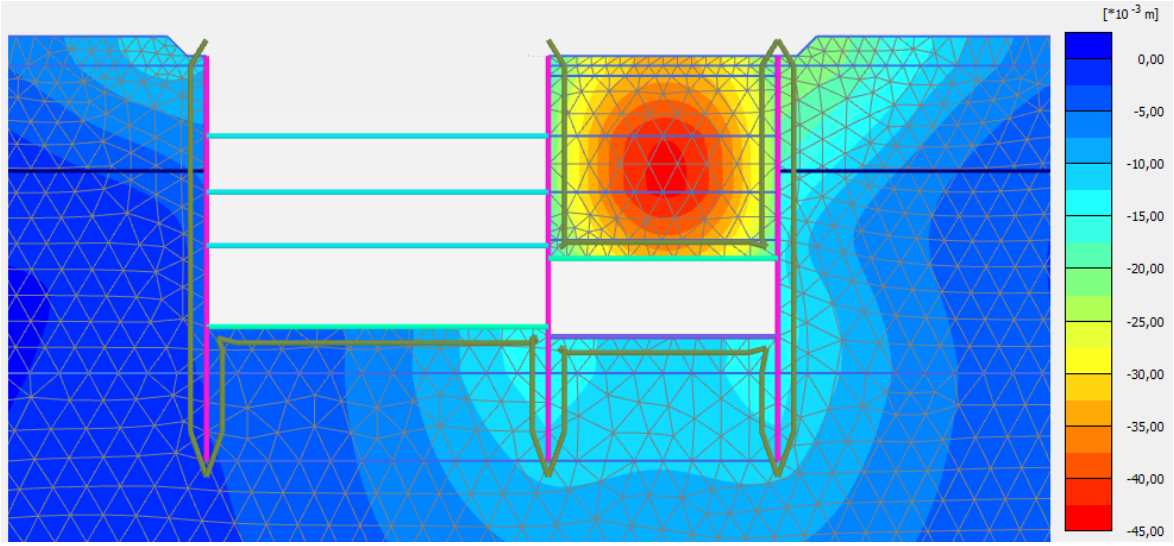

Figure 4.7 Soil displacements u_y for polystyrene concrete as backfilling material

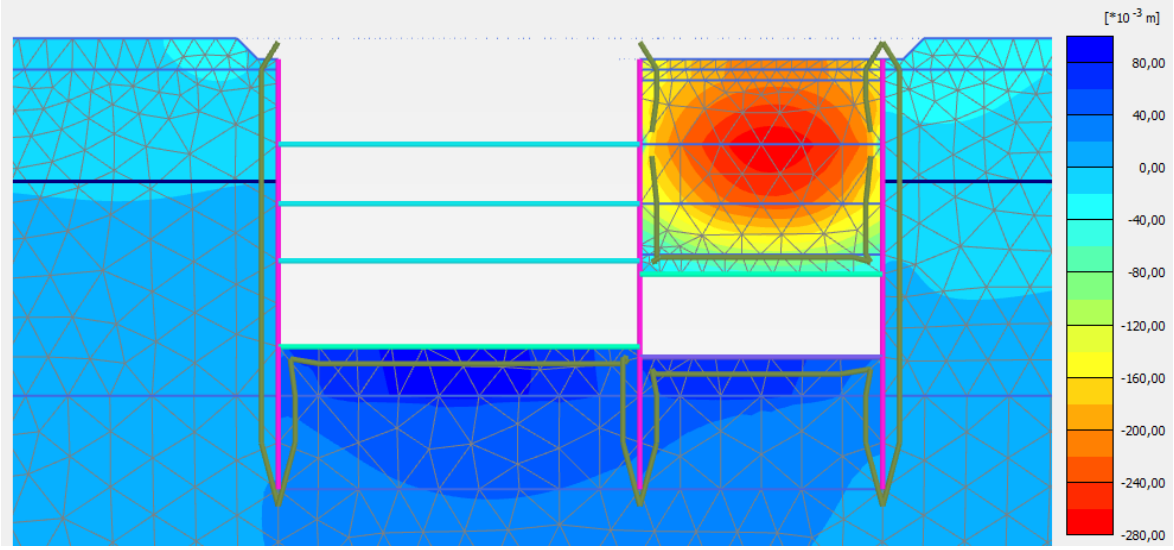

Figure 4.8 Soil displacements u_y for made ground as backfilling material

Table 4.5 Review of displacements for different backfilling materials

	Soil displacement u_y [10^{-3} m]
Soil with cement	68
Polystyrene concrete	45
Made ground	280

In case of made ground it might be possible to reduce the displacements by casting a reinforced concrete slab inside of the shaft during the backfilling phase. For purposes of this thesis a slab of a thickness 1 m was modelled in place of the second bracing level.

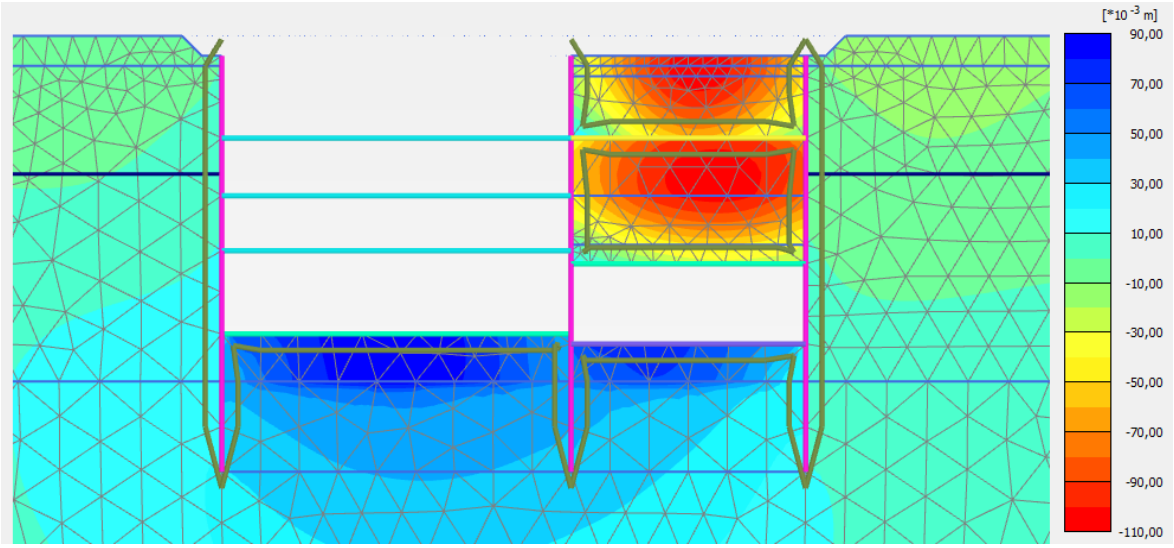

Figure 4.9 Soil displacement u_y = 0.11 m for made ground as backfilling material when concrete slab is casted inside of the shaft.

Model Outputs:

In order to be able to design the diaphragm wall affected by excavation from both sides the values of bending moments in characteristic values were taken from Plaxis. Too see the behaviour of bending moments during the phases of construction the values were put in a graph. For better transparency the graph was divided into three parts according to the construction phases.

Left sides of the graphs are the sides of MS, right sides are the sides of the shaft. You can see that in every graph the biggest moments are on the side of the shaft. In the first 7 phases there are no sharp steps in the moments' behaviour. This is because the struts inside of the shaft are connected by hinges. From Phase 8 further we can see sharp steps in the moments' behaviour due to the rigid joints between MS ceilings and diaphragm walls. This behaviour stays the same for the backfilling of the shaft. The bending moments are getting bigger with the course of construction phases. You can see in the graphs that the biggest moment is created in Phase 19 approximately in the depth of the base slab of the shaft and MS base slab.

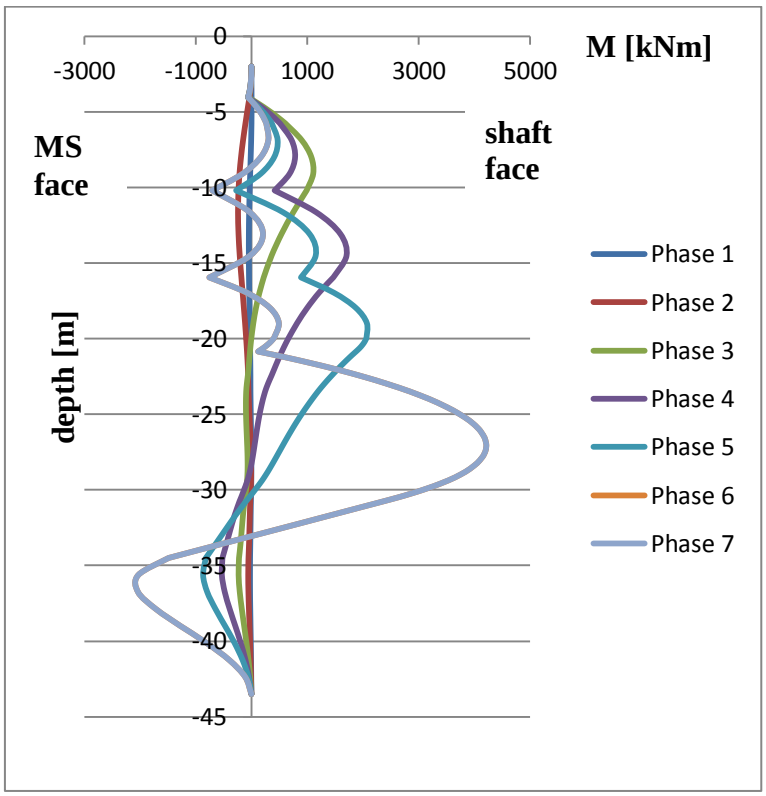

Figure 4.10 Bending moments in characteristic values Phase 1 to Phase 7

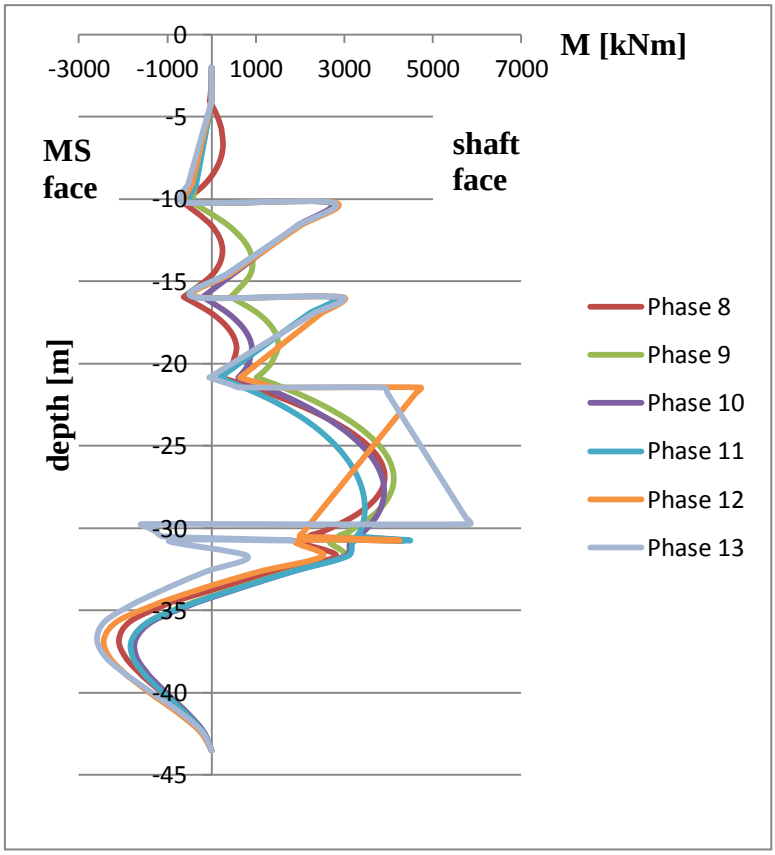

Figure 4.11 Bending moments in characteristic values Phase 8 to Phase 13

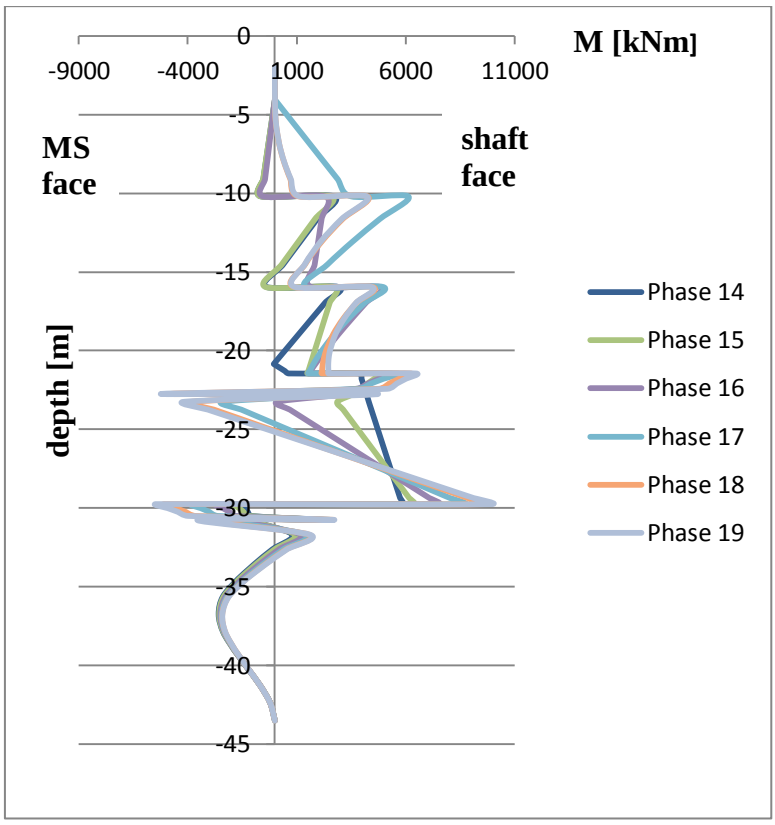

Figure 4.12 Bending moments in characteristic values Phase 14 to Phase 19

To be able to design the lateral support frame it was necessary to find the biggest normal force induced in the struts. This force is created in the 4th level of bracing system in Phase 6 and its value is -1 762 kN/m. Also it is worth notice that the 1st bracing level is in tension from Phase 9, maximum tension force is created in Phase 15 and its value is 106.4 kN/m.

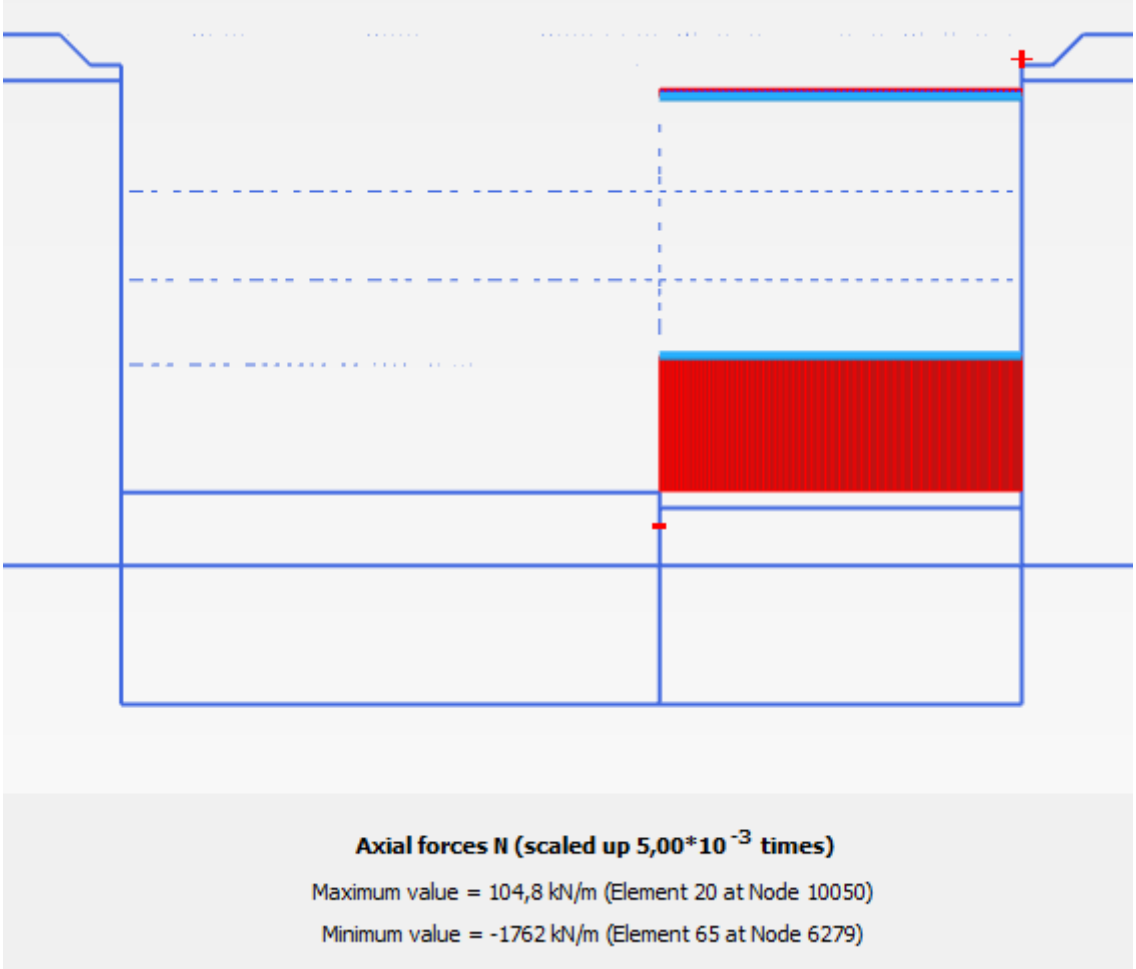

Figure 4.13 Normal forces in 1st and 4th bracing level, Phase 13

4.1.2 Mohr-Coulomb model (undrained)

The Mohr-Coulomb material model is used for all soil layers. In case of the layer of Made ground and Limestone it is set as drained, in case of layer of Clay it is set as undrained. The geometry of the model, soil and plate parameters, mesh distribution, water conditions and phases of construction remained the same as for model with CC.

Model Outputs:

The behaviour of bending moments is the same as in CC model, however the values for the right side of the wall (inside of the shaft) are bigger. The graph was again divided into three parts according to the phases of construction.

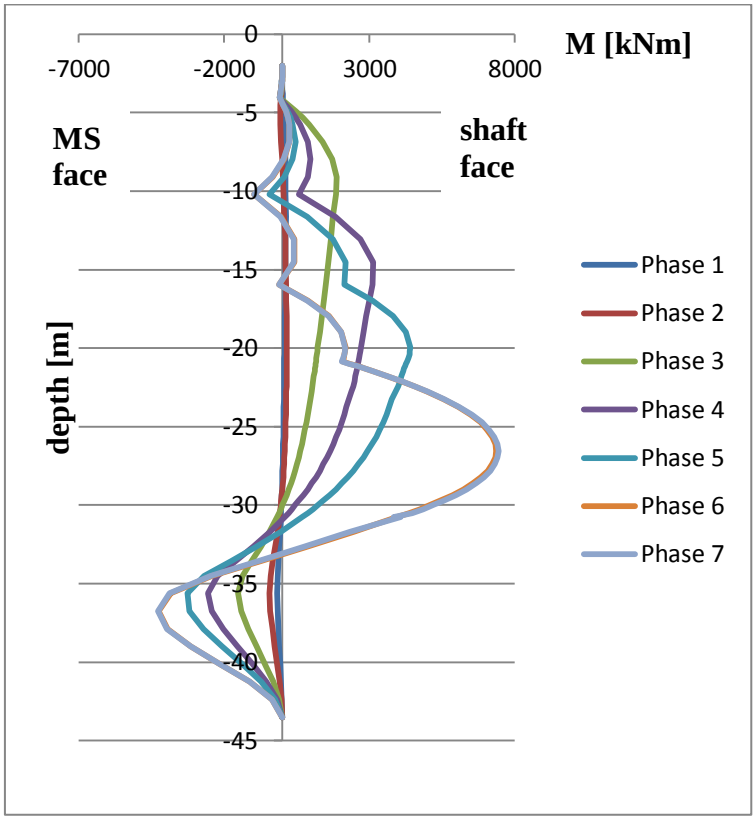

Figure 4.14 Bending moments in characteristic values Phase 1 to Phase 7

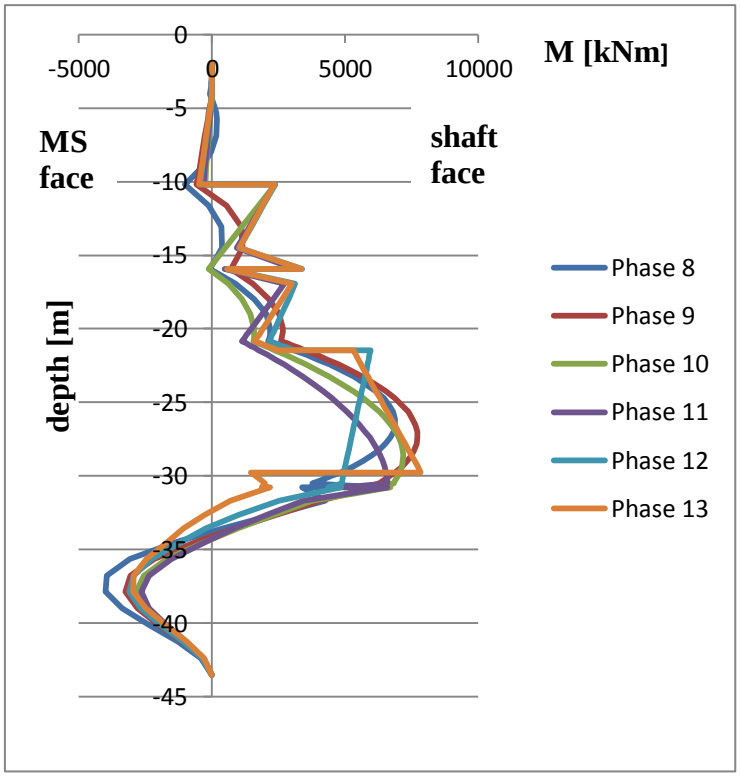

Figure 4.15 Bending moments in characteristic values Phase 8 to Phase 13

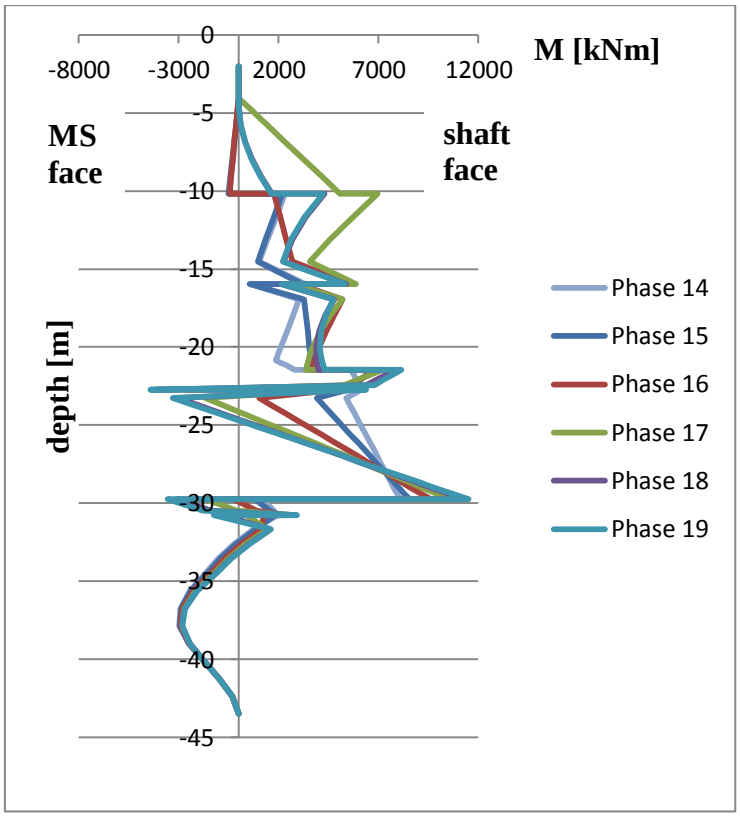

Figure 4.16 Bending moments in characteristic values Phase 14 to Phase 19

The maximum axial force in struts was created in Phase 7 and its value is -2 106 kN/m. Again from Phase 9 the 1st bracing level is in tension. The maximum value of tension is 81.24 kN/m and it is created in Phase 15.

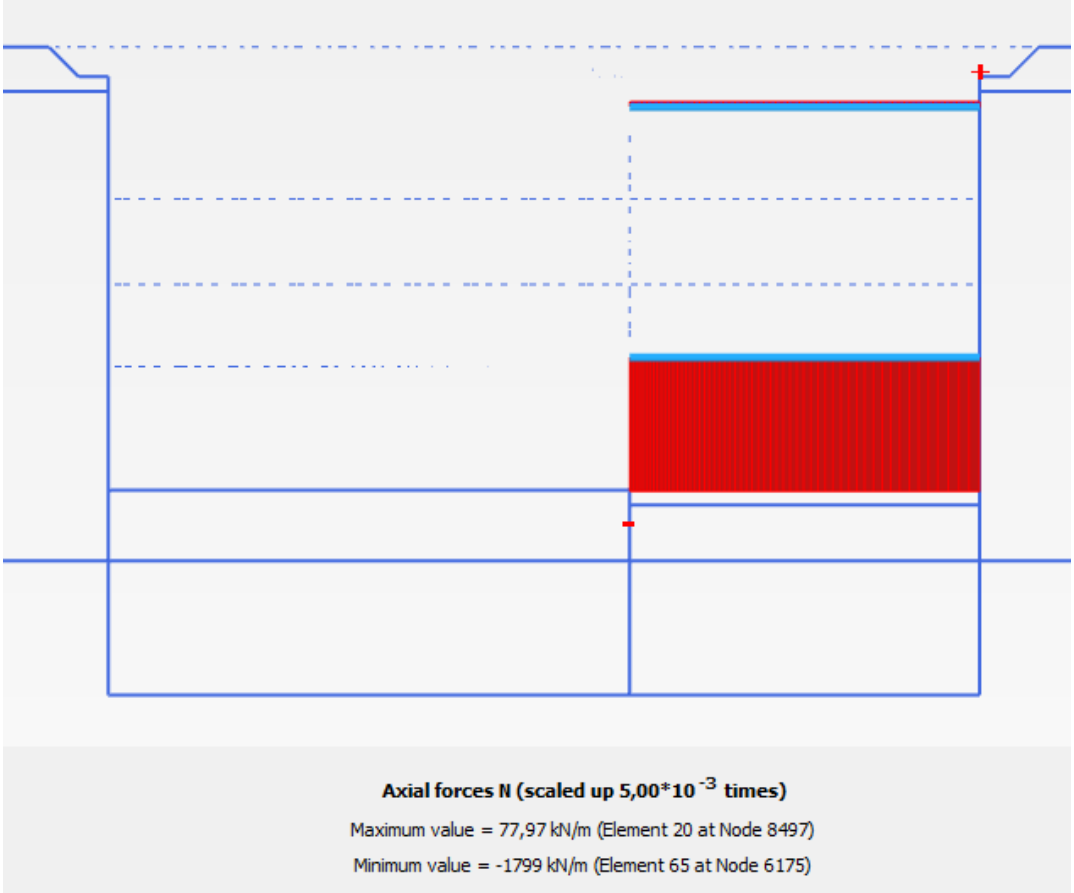

Figure 4.17 Normal forces in 1st and 4th bracing level, Phase 13

4.1.3 Comparison of CC model and MC model (undrained)

Table 4.6 Compared values of CC and MC (undrained) models

	Modified Cam Clay model	**Mohr-Coulomb model (undrained)**
Soil deformations [*10^{-3} m]		
u_x – Phase 7	36	70
u_x – Phase 13	45	90
u_x – Phase 19	25	32
u_y – Phase 13	110	100
u_y – Phase 19	68	76
Diaphragm wall deformations [*10^{-3} m]		
u_x – Phase 7	34	63
u_x – Phase 13	28	53

Bending moments on diaphragm wall [kNm/ m]		
M_{ek} – Phase 7	+4 213 -2 035	+7 439 -4 277
M_{ek} – Phase 13	+5 838 -2 588	+7 838 -2 974
M_{ek} – Phase 19	+9 961 -5 463	+11 290 -4 136
Normal forces in struts [kN/ m]		
First bracing level		
N_{ek} – Phase 7	-346	-425.7
N_{ek} – Phase 13	+104.8	+77.97
Fourth bracing level		
N_{ek} – Phase 7	-1 762	-2 106
N_{ek} – Phase 13	-1 762	-1 799

One of the main objectives of the comparison was to find out the differences in bending moments on the diaphragm wall – in its behaviour and in its values. In the graph below you can see the bending moments' envelope from MC model and CC model.

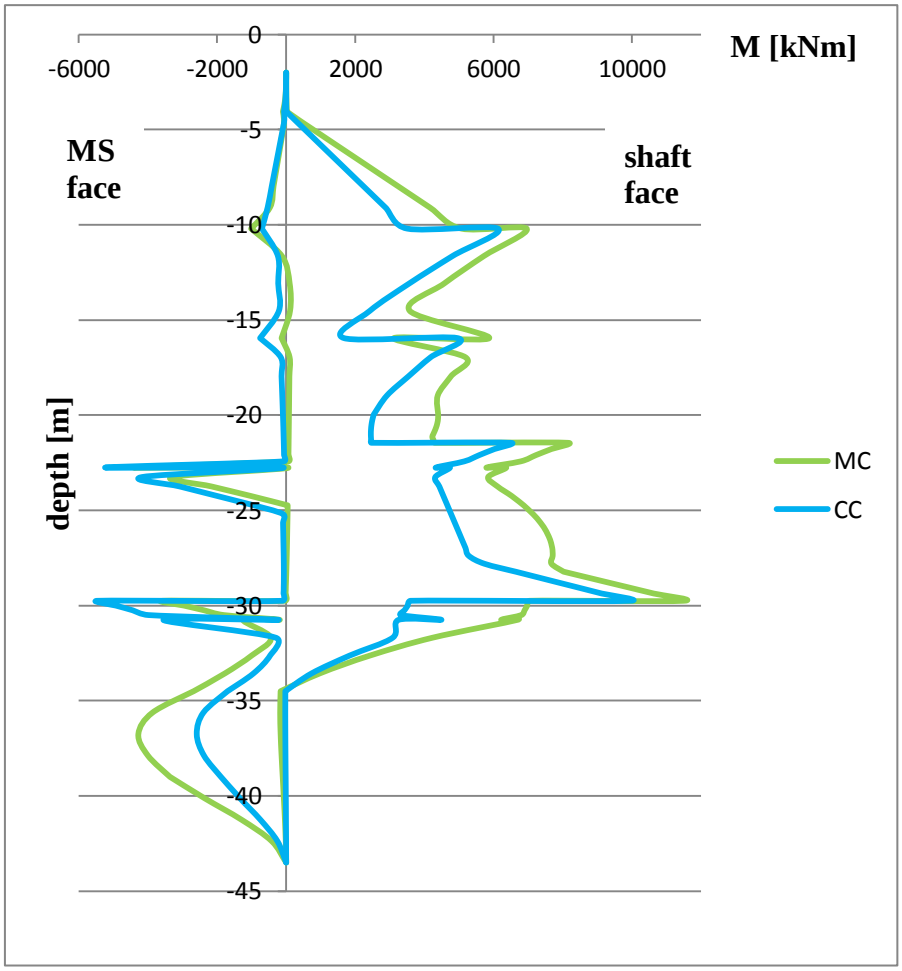

Figure 4.18 Bending moments' envelope in characteristic values

4.1.4 Mohr-Coulomb model (drained)

This model was created for the possibility of comparison between Geo5 model and Plaxis model. All soil layers are modelled by MC material model and they are set as drained. The geometry of the model, soil and plate parameters, mesh distribution and water conditions remained the same as for MC (undrained).

Model Outputs:

The behaviour of bending moments is displayed at the right wall of the shaft (left side of the graph is the inner side of the shaft, right side is the side that remains covered with soil).

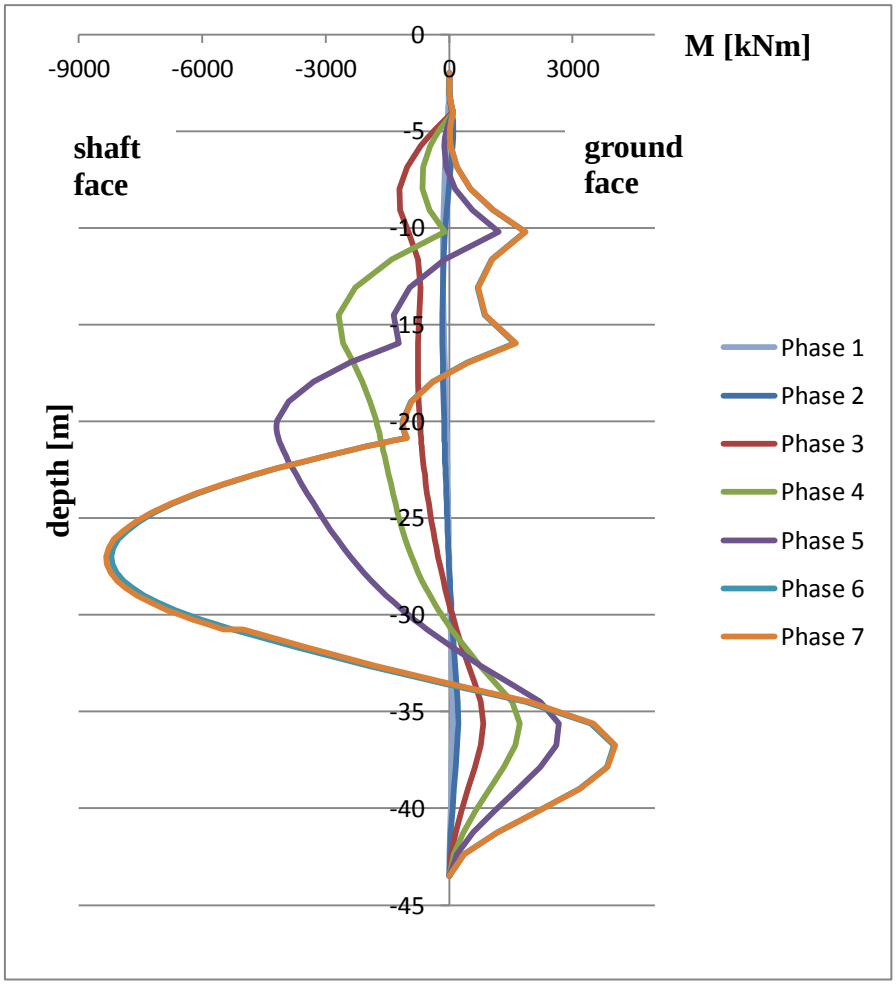

Figure 4.19 Bending moments in characteristic values Phase 1 to Phase 7

4.2 Geo5

4.2.1 Model with effective parameters

The model "Sheeting check" was used to determine loads on the diaphragm wall. The bedding reaction method is set as a calculation process in this mode. This means that the earth loads are dependent on the deformations of the bracing structure and on the deformation of soils and the other way around.

The Eurocode 2 was set for the reinforced concrete diaphragm wall and the Eurocode 7 – design approach 2 was set for the soils.

Modulus of subgrade reaction was calculated according to Schmitt:

$$k_h = 2.1 * \frac{{E_{oed}}^{4/3}}{(EI)^{1/3}}$$

Table 4.7 Modulus of subgrade reaction for different layers

	Made ground	Clay	Limestone
k_h (Geo)	3.11	16.3	248.74

All soil/rock layers are set in effective parameters (values are stated in Table 2.1).

Structural parameters:

A = 1.5 m^2/m
I = 0.281 m^4/m
E = 33 GPa
G = 13.75 GPa

The lateral support frame in Geo5 is given by the area of one strut, its length, modulus of elasticity and distance between struts. For comparison in Plaxis the bracing frame is given by the length of a strut, modulus of elasticity and average area and average moment of inertia of struts per one meter. Considering the structural arrangement of the bracing frame in 3D, it is not fully possible to convert its behaviour to 2D. Therefore the 3D model in Scia Engineer is used for design of the lateral support frame.

Phases of construction:

In Geo5 it is not possible to simulate the excavation from both sides of the diaphragm wall; therefore the phases of construction in the model are finished when the process of works gets to the casting of the base slab of the shaft (Phase 7 in Plaxis). The process of excavation, bracing and dewatering is set the same way as in Plaxis.

Phase 1: excavation to the 1st bracing level
Phase 2: excavation to the 2nd bracing level, activation of the 1st bracing level
Phase 3: excavation to the 3rd bracing level, activation of the 2nd bracing level
Phase 4: excavation to the 4th bracing level, activation of the 3rd bracing level
Phase 5: excavation to the level of base slab, activation of the 4th bracing level
Phase 6: activation of base slab

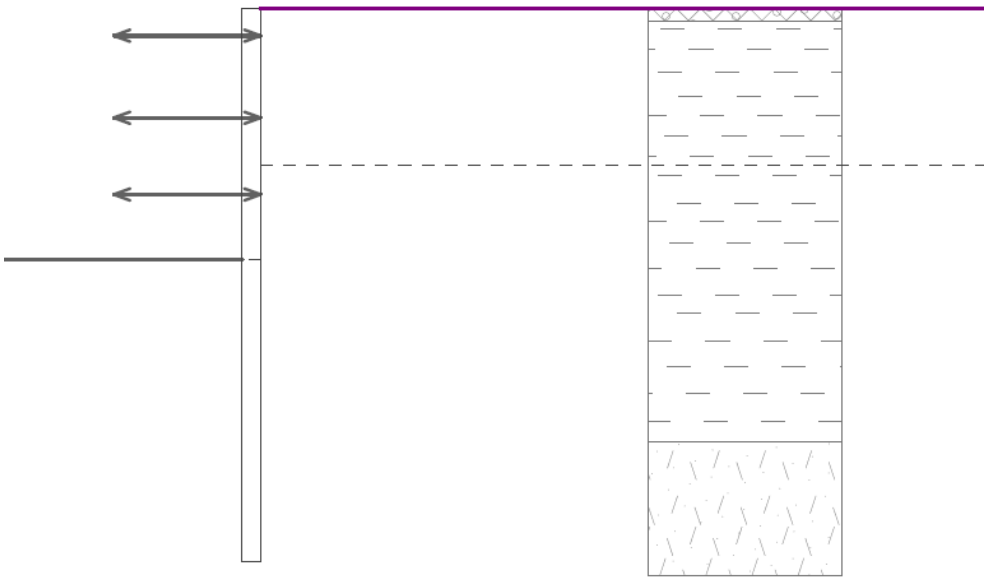

Figure 4.20 Phase 4

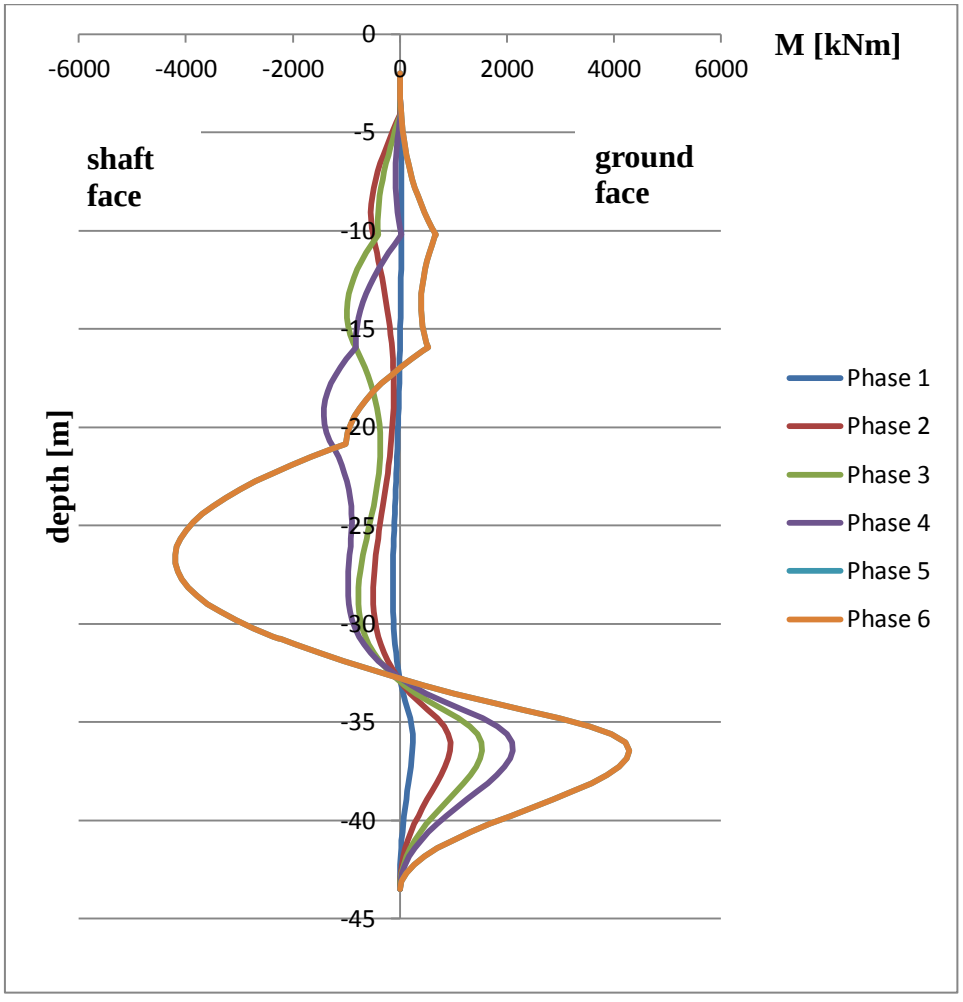

Figure 4.21 Bending moments in characteristic values Phase 1 to Phase 6

4.2.2 Comparison of MC model (drained) and Geo5 model

Table 4.8 Comparison of MC model (drained) and Geo5 model

	MC model (drained)	Geo5 Model
max positive bending moment $+M_{ek}$ [kNm/m]	+4 042	+4 286
max negative bending moment $-M_{ek}$ [kNm/m]	-8 334	-4 200
max wall displacement u_x [mm]	58.37	24.4

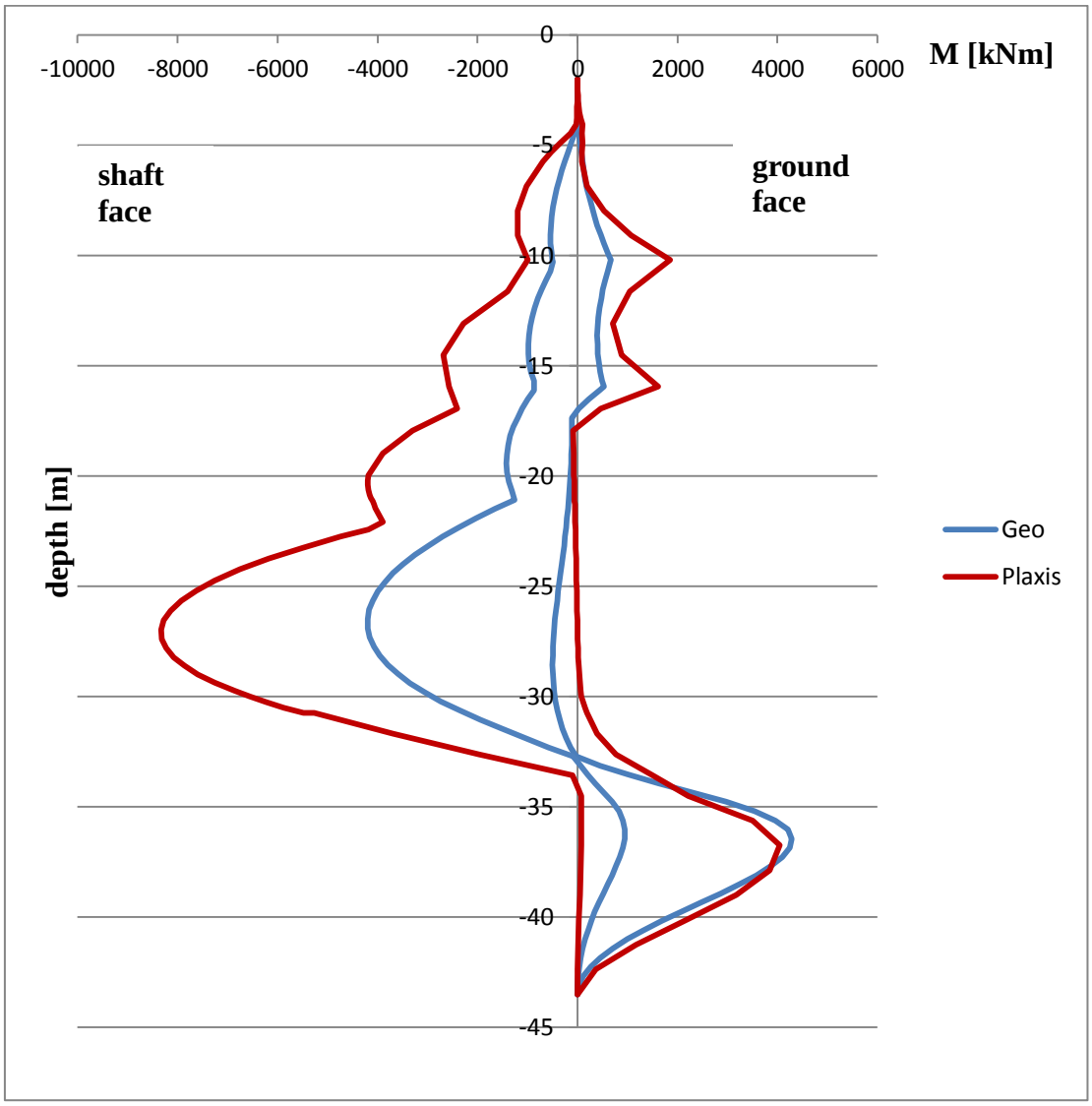

Figure 4.22 Bending moments' envelopes in characteristic values

4.2.3 Comparison of CC model (undrained), MC model (undrained) and MC model (drained)

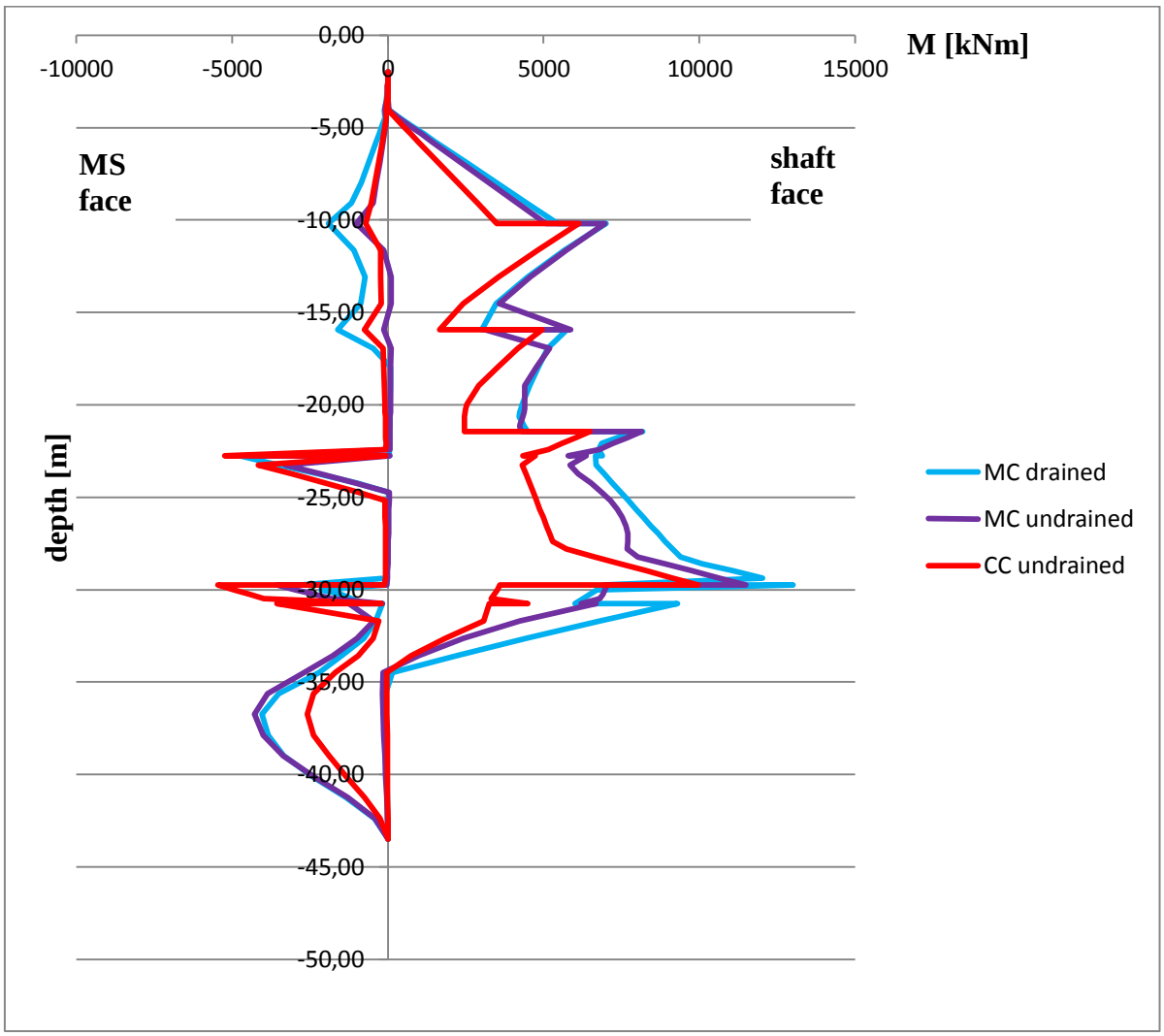

Figure 4.23 Comparison of bending moments' envelopes in characteristic values

4.3 Scia Engineer

The lateral support frame is modelled in software Scia Engineer by its half. It is supported in line in vertical axis z. There are support conditions set for x and y axis in the middle of the length of the waler beam and therefore it is not necessary to model the whole frame. The struts are connected to waler beam by hinges.

The frame is loaded by its own weight and by horizontal force taken from software Plaxis. This force is the biggest force created in struts during the phases of construction according to Plaxis and its value is 1 762 kN/m (taken from CC model (undrained)).

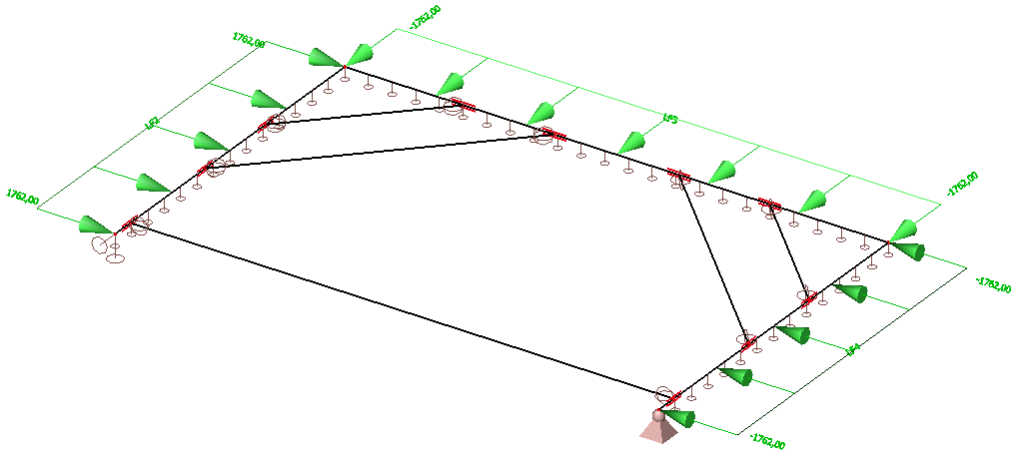

Figure 4.24Model of bracing frame in Scia Engineer

The components are modelled by its real cross sectional shapes. The section of the waler beam is twisted by 90 degrees in the model.

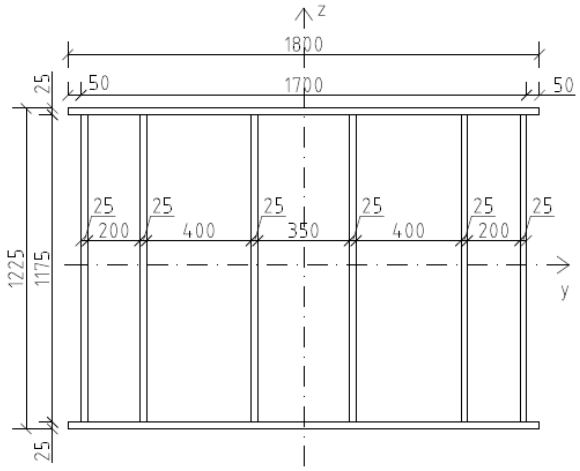

Figure 4.25 Cross section of the waler beam

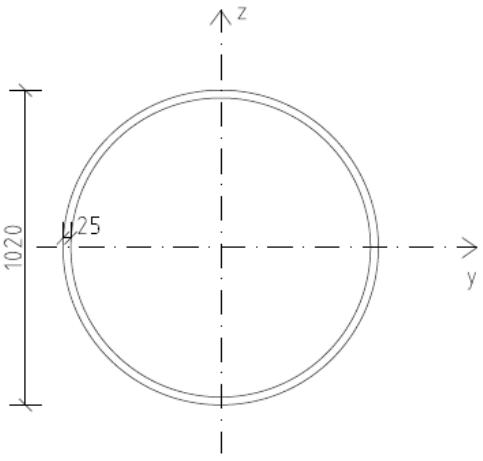

Figure 4.26 Cross section of struts

Table 4.9 Cross sectional parameters

	Waler beam	**Strut**
A [m^2]	0.26625	$7.8147*10^{-2}$
I_y [m^4]	$5.2683*10^{-2}$	$9.6771*10^{-3}$
I_z [m^4]	$8.9623*10^{-2}$	$9.6771*10^{-3}$
$W_{pl,y}$ [m^3]	0.10577	$2.4756*10^{-2}$
$W_{pl,z}$ [m^3]	0.1367	$2.4756*10^{-2}$
Steel	S235	S355
f_y [MPa]	235	355

For sketch of lateral support frame see Appendix 8.

Model outputs:

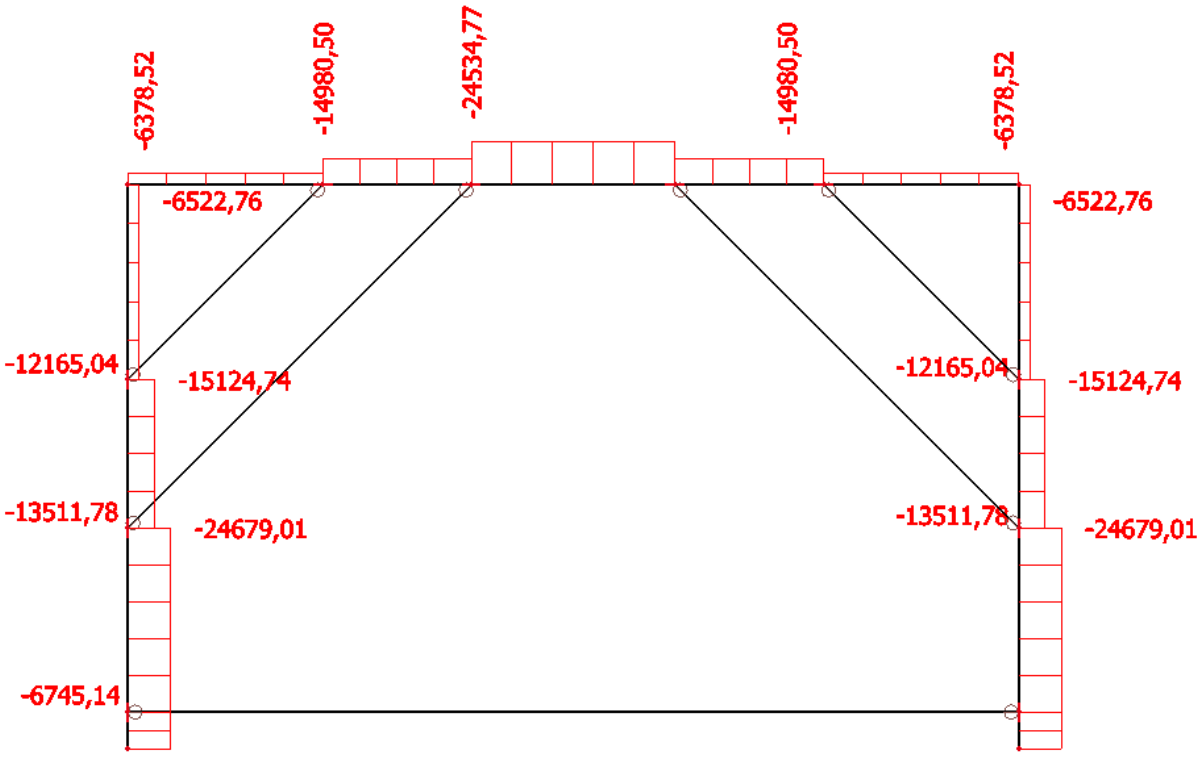

Figure 4.27 Design values of normal forces N_{Ed} from combination of self-weight and forces induced in frame during construction phases

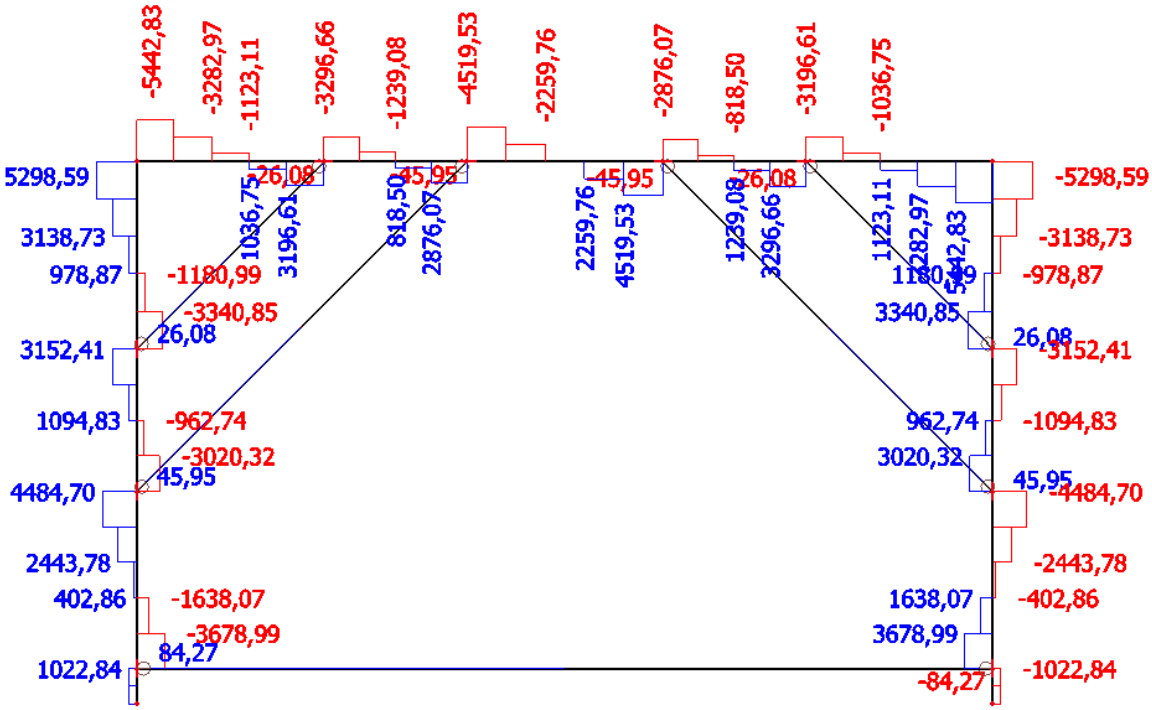

Figure 4.28 Design values of shear forces $V_{Ed,z}$ from combination of self-weight and forces induced in frame during construction phases

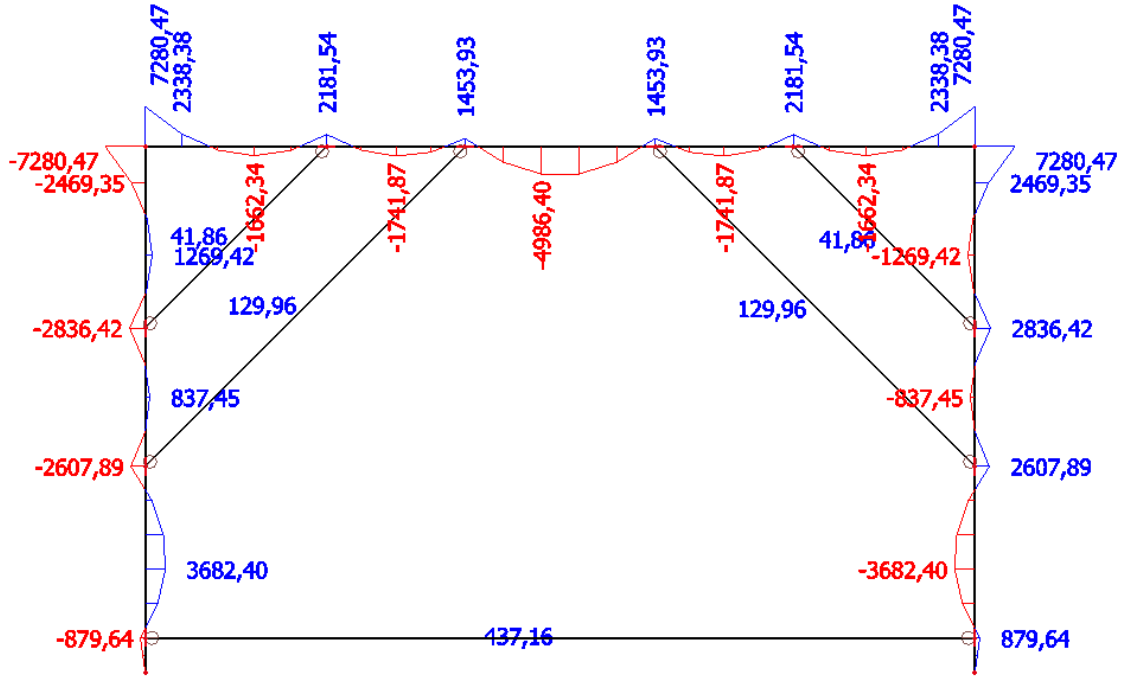

Figure 4.29 Design values of bending moments $M_{Ed,y}$ from combination of self-weight and forces induced in frame during construction phases

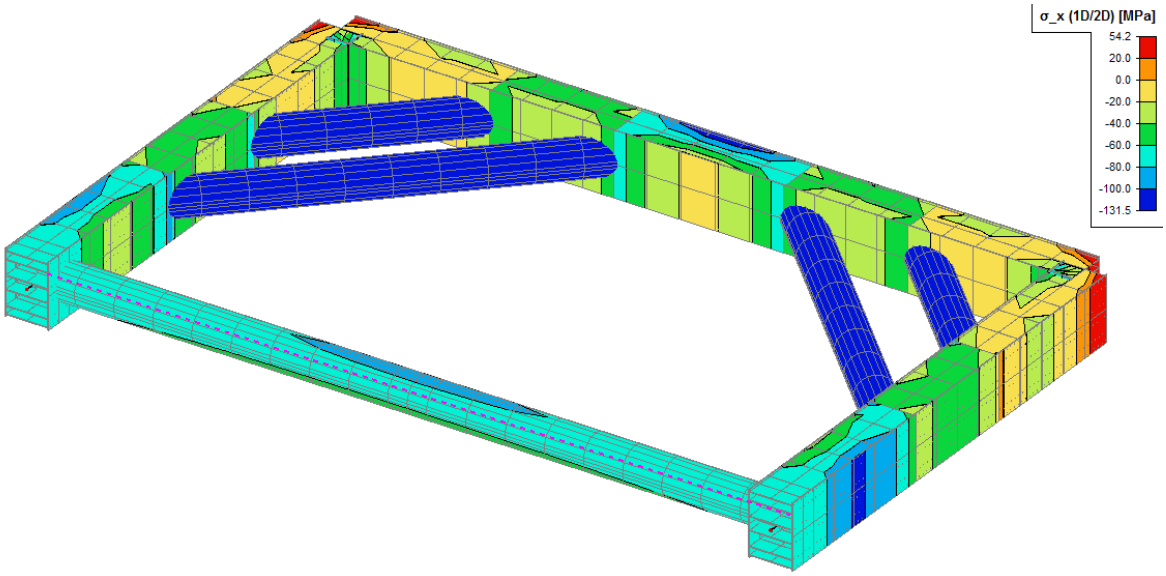

Figure 4.30 Stress σ_x in the bracing frame – the most stressed parts are displayed in figure by dark blue and red colour, these parts are subjected to design check in Chapter 4.5

4.4 Design of diaphragm wall affected by excavation from both sides

The design of the diaphragm wall was carried out according to Eurocodes: the design of the concrete structural parts was carried out according to Eurocode 2 [9] and the geotechnical parameters were established according to Eurocode 7 – design approach 2 [10].

In this thesis only ground pressure was considered. It is obvious that in reality there would be surface surcharge from construction site installations and variable loads from the construction machines (especially during TBM lowering). Also it would be necessary to evaluate the seismic effects.

Concrete grade C35/45 was specified for the whole structure and the reinforcement steel B500B was taken for the diaphragm walls.

Concrete grade C35/45

$f_{ck} = 35\ MPa$

$f_{cd} = \alpha_{cc} * f_{ck} / \gamma_c = 1.0*35/1.5 = 23.33\ MPa$

$f_{cm} = 43\ MPa$

$E_{cm} = 33.5\ GPa$

$\lambda = 0.8$

$\eta = 1$

$\varepsilon_{cu3} = 3.5$ ‰

Reinforcement - Steel B500B

$f_{yk} = 500$ MPa

$f_{yd} = f_{yk} / \gamma_s = 500/1.15 = 434.78$ MPa

$E_s = 200$ GPa

$\varepsilon_{yd} = f_{yd} / E_s = 2.17$ ‰

A bending moment envelope in characteristic values was obtained from the Plaxis model that uses Modified Cam Clay material model for clay. According to EC 7 – design approach 2 [10] these values where multiplied by $\gamma_G = 1.35$ to obtain the design values. The reinforcement was designed to the bending moments' envelope in design values. The reinforcement bars of a diameter 25 mm and 40 mm were chosen for the structure. The spacing is 140 mm in case of one, two and three rows of reinforcement and in case of the fourth row of reinforcement it is 420 mm.

The wall is mostly loaded on the inner side of the shaft. The biggest moments are created when the shaft is backfilled. In order to cover the design bending moments but on the other hand to stay economical there are multiple schemes of reinforcement changing with the depth of the wall.

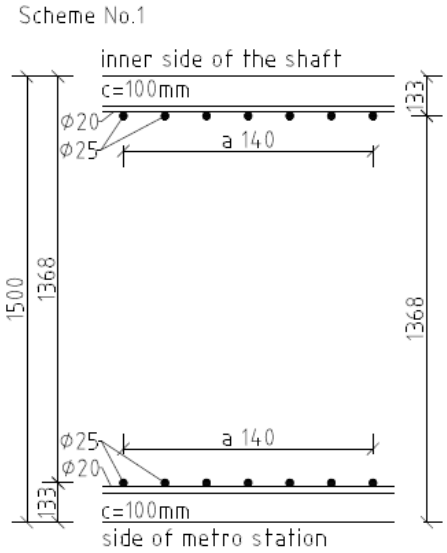

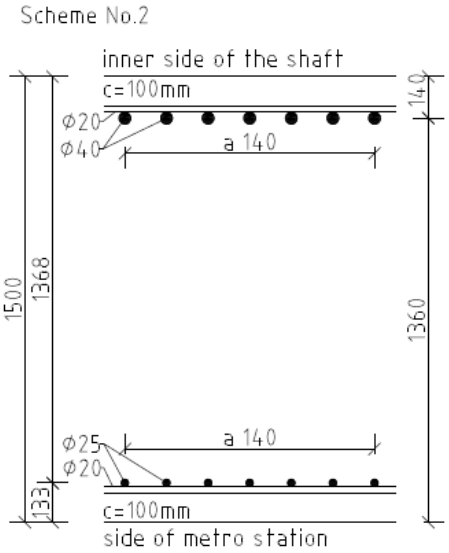

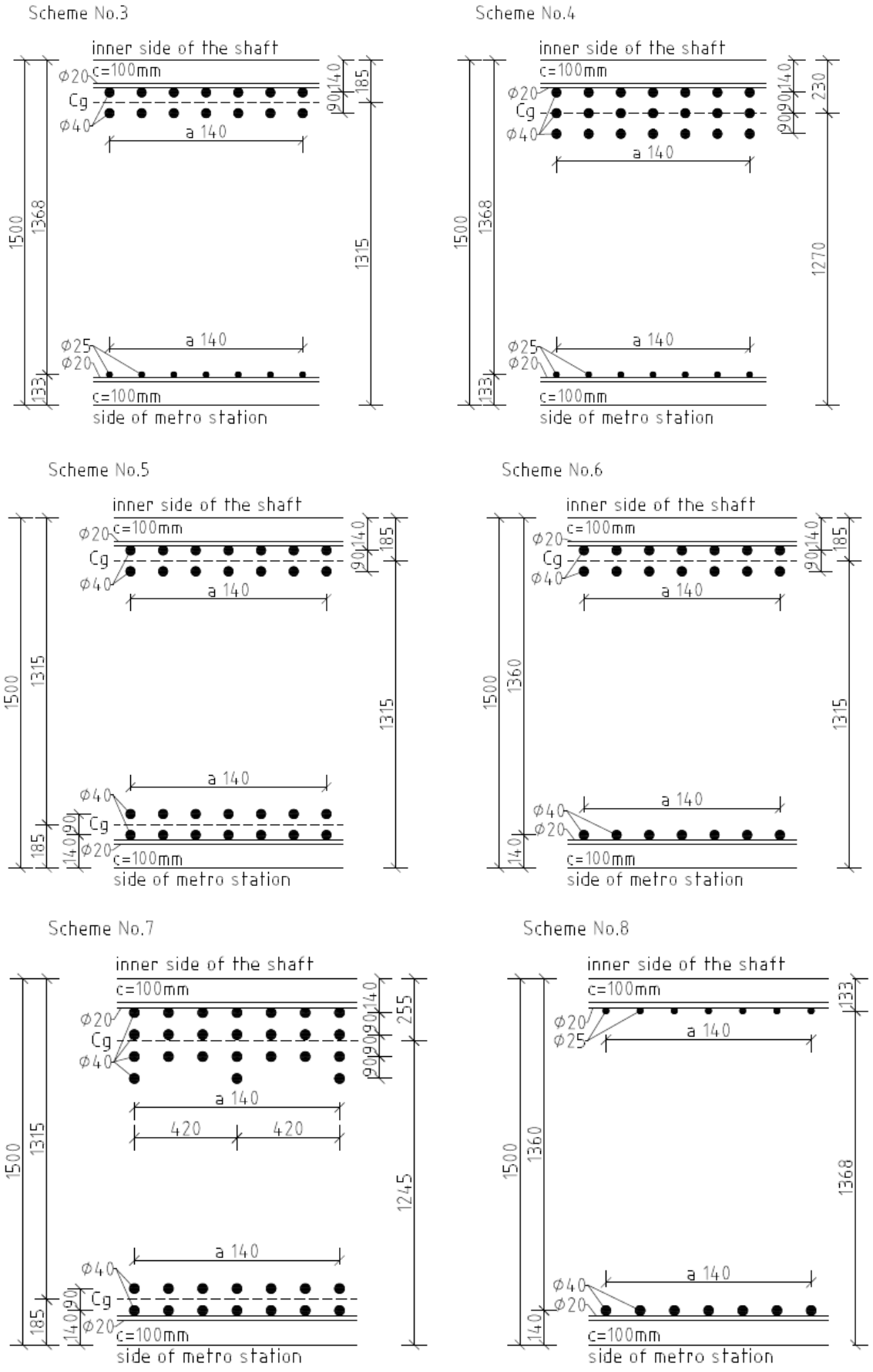

Figure 4.31 Reinforcement schemes

Calculation:

$A_{s,rqd} = b * d * f_{cd} / f_{yd} * \sqrt{1 - 2 * M_{ed}/(b * d^2 * f_{cd})}$

$x = A_{s,prov} * f_{yd} / (b * f_{cd} * \lambda)$

$z = d - 0.5 * \lambda * x$

$M_{rd} = A_{s,prov} * z * f_{yd}$

$b = 1.0\ m$

$h = 1.5\ m$

$c = 100\ mm$

Where more layers of reinforcement were used, effective depth "*d*" was taken from the centre of gravity of the reinforcement (calculated by weighted average).

There are two solutions for reinforcement carried out in this thesis. First solution would be more efficient considering the amount of used reinforcement. However it would not be very practical because of the assembly on the construction site. Second solution is less economical but it would be easier to assemble.

Find the values of calculation in Appendix 6 and Appendix 7.

Check of structural principles:

$A_{s,v\,min} = 0.002 * A_c = 0.002 * 1.5 * 1.0 = 30.00 * 10^{-4}\ m^2$ *ok*

$A_{s,v\,max} = 0.04 * A_c = 0.04 * 1.5 * 1.0 = 600.00 * 10^{-4}\ m^2$ *ok*

$s_{max} \leq 3 * h = 3 * 1500 = 4500\ mm$ *ok*

$\leq 400\ mm$ *ok*

$s_{min} \geq max\ \{1.2*\Phi;\ d_g + 5\ mm;\ 20\ mm\}$

$\geq max\ \{1.2*40;\ 16 + 5\ mm;\ 20\ mm\}$

$\geq max\ \{1.2*40;\ 16 + 5\ mm;\ 20\ mm\}$

$\geq 48\ mm$ *ok*

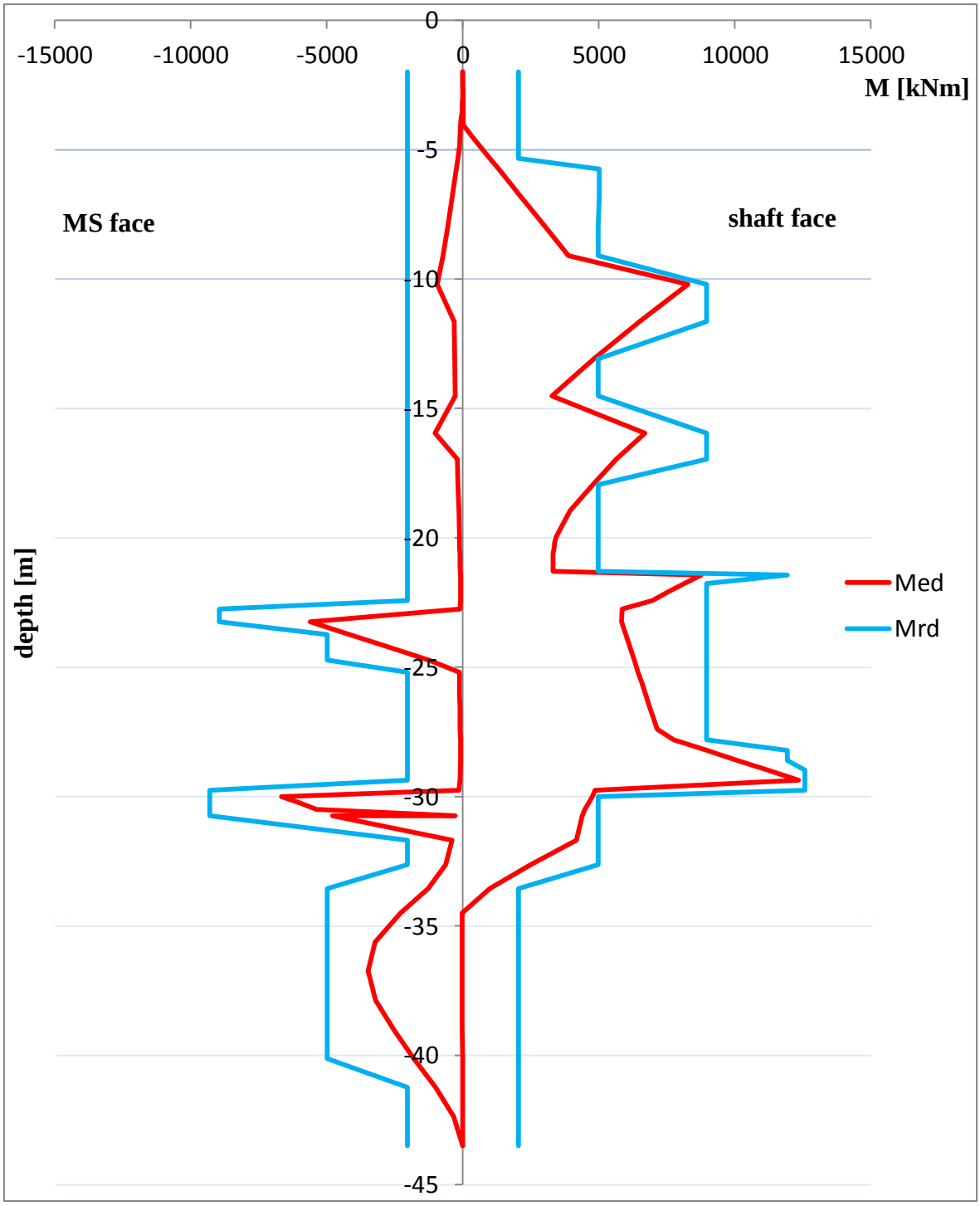

Figure 4.32 First solution - Envelope of bearing and design moments. Reinforcement schemes change frequently.

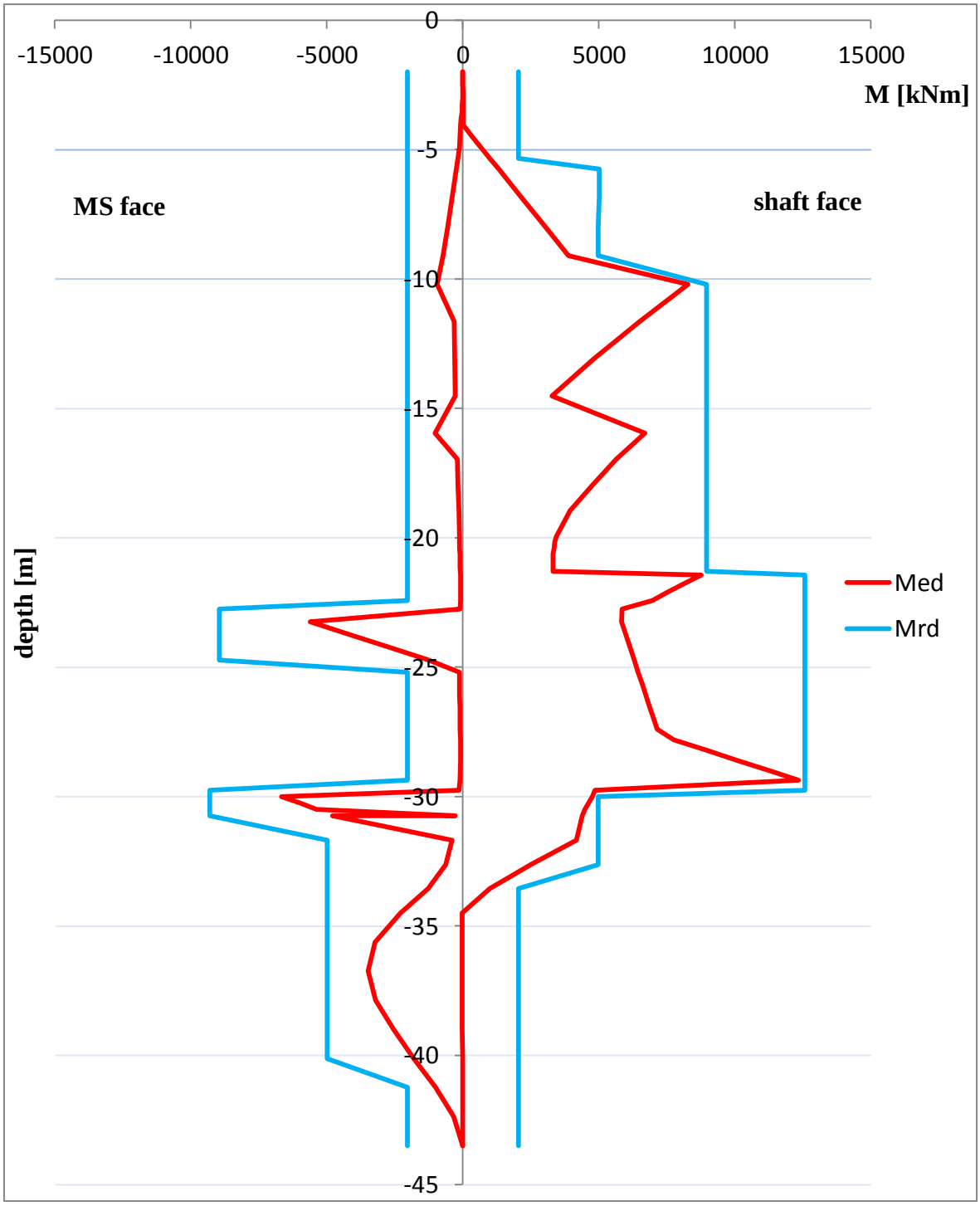

Figure 4.33 Second solution - Envelope of bearing and design moments. Reinforcement schemes do not change so often on the length of the wall.

4.5 Design of lateral support frame

For the design check of the steel bracing the 4th level of lateral support system was chosen. Parameters for waler beam and for strut were taken from Scia Engineer.

4.5.1. Design check of the waler beam

Design values of inner forces were taken from Scia Engineer.

Maximum loads:

$N_{Ed,max} = 24\ 679.01\ kN$ ($M_{eq} = 3\ 682.40\ kNm$, $V_{eq} = 1\ 638.07\ kN$)

$V_{Ed,max} = 5\ 442.83\ kN$

$M_{Ed,max} = 7\ 280.47\ kNm$ ($N_{eq} = 6\ 522.76\ kN$, $V_{eq} = 5\ 442.83\ kN$)

According to EC 3 [11] the section of waler beam is class 1.

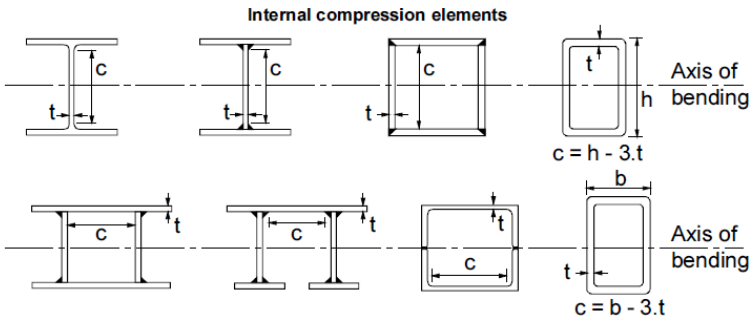

Figure 4.34 Cross sectional classification [11]

$$\frac{c}{t} = \frac{350}{25} = 14 \leq 33\varepsilon = 33 \quad ok$$

$$\varepsilon = \sqrt{\frac{235}{f_y}} = \sqrt{\frac{235}{235}} = 1.0$$

1. Compression ($N_{Ed,max} = 24\ 679.01\ kN$)

Bearing capacity:

$$N_{C,Rd} = \frac{A * f_y}{\gamma_{m0}} = \frac{0.26625 * 235 * 10^6}{1.0} = 62\ 568.75\ kN$$

Limit condition:

$$\frac{N_{Ed,max}}{N_{C,Rd}} = \frac{24\ 679.01}{62\ 568.75} = 0.39 \leq 1.0$$

2. Shear ($V_{Ed,max}$ = *5 442.83 kN*)

Bearing capacity:

$$V_{pl,Rd} = \frac{A_v * (\frac{f_y}{\sqrt{3}})}{\gamma_{m0}} = \frac{0.176 * (235 * \frac{10^6}{\sqrt{3}})}{1.0} = 23\,879.20\ kN$$

Shearing area:

$$A_v = \eta * (h_{wi} * t_{wi}) = 1.0 * 1.175 * 0.025 * 6 = 0.176$$

Limit condition:

$$\frac{V_{max}}{V_{pl,Rd}} = \frac{5\,442.83}{23\,879.20} = 0.23\ \leq 1.0$$

Because the ratio of V_{max} and $V_{pl,Rd}$ is smaller than 0.5 it is possible to neglect the effects of shear forces for design check of interaction between bending moments, shear forces and normal forces and it is not necessary to reduce the yield stress.

3. Bending ($M_{Ed,y,max}$= *7 280.47 kNm*)

Bearing capacity:

$$M_{pl,Rd,y} = \frac{W_{pl,y} * f_y}{\gamma_{m0}} = \frac{0.10577 * 235 * 10^6}{1.0} = 24\,855.95\ kNm$$

Limit condition:

$$\frac{M_{Ed,y,max}}{M_{pl,Rd,y}} = \frac{7\,280.47}{24\,855.95} = 0.29\ \leq 1.0$$

4. Buckling

- **y axis**

Buckling capacity:

$$N_{b.Rd,y} = \frac{\chi_y * A * f_y}{\gamma_{m1}} = \frac{1.0 * 0.26625 * 235 * 10^6}{1.0} = 62\,568.75\ kN$$

Buckling coefficient:

$$\chi_y = \frac{1}{\emptyset_y + \sqrt{{\emptyset_y}^2 - {\lambda_y}^2}} = \frac{1}{0.48 + \sqrt{0.48^2 - 0.072^2}} = 1.05 \leq 1.0 \rightarrow\ \chi_y = 1.0$$

$$\emptyset_y = 0.5 * \left[1 + \alpha * \left(\lambda_y - 0.2\right) + {\lambda_y}^2\right] = 0.5 * [1 + 0.34 * (0.072 - 0.2) + 0.072^2] = 0.48$$

where α is coefficient of imperfection (buckling curve "b" → $\alpha = 0.34$)

Relative slenderness:

$$\lambda_y = \sqrt{\frac{A * f_y}{N_{cr,y}}} = \sqrt{\frac{0.26625 * 235 * 10^6}{12.11 * 10^9}} = 0.072$$

Critical force:

$$N_{cr,y} = \pi^2 * \frac{E * I_y}{{L_{cr}}^2} = \pi^2 * \frac{210 * 10^9 * 5.2683 * 10^{-2}}{3.003^2} = 12.11 * 10^9\ N$$

Critical length:

$$L_{cr} = 0.7 * L = 0.7 * 4.29 = 3.003\ m$$

Limit condition:

$$\frac{N_{Ed,max}}{N_{b,Rd,y}} = \frac{24\ 679.01}{62\ 568.75} = 0.39 \leq 1.0 \qquad ok$$

- **z axis**

Buckling capacity:

$$N_{b.Rd,z} = \frac{\chi_z * A * f_y}{\gamma_{m1}} = \frac{1.0 * 0.26625 * 235 * 10^6}{1.0} = 62\ 568.75\ kN$$

Buckling coefficient:

$$\chi_z = \frac{1}{\emptyset_z + \sqrt{{\emptyset_z}^2 - {\lambda_z}^2}} = \frac{1}{0.477 + \sqrt{0.477^2 - 0.055^2}} = 1.05 \leq 1.0 \rightarrow\ \chi_z = 1.0$$

$$\emptyset_z = 0.5 * \left[1 + \alpha * (\lambda_z - 0.2) + {\lambda_z}^2\right] = 0.5 * [1 + 0.34 * (0.055 - 0.2) + 0.055^2] = 0.477$$

where α is coefficient of imperfection (buckling curve "b" → $\alpha = 0.34$)

Relative slenderness:

$$\lambda_z = \sqrt{\frac{A * f_y}{N_{cr,z}}} = \sqrt{\frac{0.26625 * 235 * 10^6}{20.6 * 10^9}} = 0.055$$

Critical force:

$$N_{cr,z} = \pi^2 * \frac{E * I_z}{{L_{cr}}^2} = \pi^2 * \frac{210 * 10^9 * 8.9623 * 10^{-2}}{3.003^2} = 20.6 * 10^9\ N$$

Critical length:

$$L_{cr} = 0.7 * L = 0.7 * 4.29 = 3.003\ m$$

Limit condition:

$$\frac{N_{Ed,max}}{N_{b,Rd,z}} = \frac{24\ 679.01}{62\ 568.75} = 0.39 \leq 1.0 \qquad ok$$

5. Bending + Buckling

Interaction taken for $N_{Ed,max}$=*24 679.01 kN* and M_{eq}=*3 682.40 kNm*.

- **y axis**

Limit condition:

$$\frac{N_{Ed}}{\frac{\chi_y * N_{Rk}}{\gamma_{m1}}} + k_{yy} * \frac{M_{y,Ed} + \Delta M_{y,Ed}}{\frac{\chi_{LT} * M_{y,Rk}}{\gamma_{m1}}} + k_{yz} * \frac{M_{z,Ed} + \Delta M_{z,Ed}}{\frac{M_{z,Rk}}{\gamma_{m1}}} \leq 1.0$$

where:

$\Delta M_{y,Ed} = \Delta M_{z,Ed} = 0\ kNm$

$M_{z,Ed} = 0\ kNm\ (caused\ only\ by\ self\ weight, small\ value\ possible\ to\ neglect)$

$\chi_{LT} = 1.0$

$N_{Rk} = f_y * A = 235 * 10^6 * 0.26625 = 62\ 568.75\ kN$

$M_{y,Rk} = f_y * W_{Pl,y} = 235 * 10^6 * 0.10577 = 24\ 855.95\ kNm$

$M_{z,Rk} = f_y * W_{Pl,z} = 235 * 10^6 * 0.1367 = 32\ 124.5\ kNm$

Values of k_{yy}, k_{yz}, k_{zy}, k_{zz} are taken according to Annex B of EC 3 [11] (simplified method).

$$k_{yy} = C_{my} * \left(1 + (\lambda_y - 0.2) * \frac{N_{Ed}}{\frac{\chi_y * N_{Rk}}{\gamma_{m1}}}\right)$$

$$= 0.9 * \left(1 + (0.072 - 0.2) * \frac{24\ 679.01}{\frac{1.0 * 62\ 568.75}{1.0}}\right) = 0.85$$

$$\leq C_{my} * \left(1 + 0.8 * \frac{N_{Ed}}{\frac{\chi_y * N_{Rk}}{\gamma_{m1}}}\right) = 1.18 \quad ok$$

$C_{my} = 0.9$

$k_{yz} = 0.6 * k_{zz} = 0.6 * 0.85 = 0.51$

$C_{mz} = 0.9$

$$k_{zz} = C_{mz} * \left(1 + (\lambda_z - 0.2) * \frac{N_{Ed}}{\frac{\chi_z * N_{Rk}}{\gamma_{m1}}} \right)$$

$$= 0.9 * \left(1 + (0.055 - 0.2) * \frac{24\ 679.01}{\frac{1.0 * 62\ 568.75}{1.0}} \right) = 0.85$$

$$\leq C_{mz} * \left(1 + 0.8 * \frac{N_{Ed}}{\frac{\chi_z * N_{Rk}}{\gamma_{m1}}} \right) = 1.18 \quad ok$$

Limit condition:

$$\frac{24\ 679.01}{\frac{1.0 * 62\ 568.75}{1.0}} + 0.85 * \frac{3\ 682.4 + 0}{\frac{1.0 * 24\ 855.95}{1.0}} + 0 = 0.52 \leq 1.0 \qquad ok$$

- **z axis**

$$\frac{N_{Ed}}{\frac{\chi_z * N_{Rk}}{\gamma_{m1}}} + k_{zy} * \frac{M_{y,Ed} + \Delta M_{y,Ed}}{\frac{\chi_{LT} * M_{y,Rk}}{\gamma_{m1}}} + k_{zz} * \frac{M_{z,Ed} + \Delta M_{z,Ed}}{\frac{M_{z,Rk}}{\gamma_{m1}}} \leq 1.0$$

$k_{zy} = 0.6 * k_{yy} = 0.6 * 0.85 = 0.51$

Limit condition:

$$\frac{24\ 679.01}{\frac{1.0 * 62\ 568.75}{1.0}} + 0.51 * \frac{3\ 682.4 + 0}{\frac{1.0 * 24\ 855.95}{1.0}} + 0 = 0.52 \leq 1.0 \qquad ok$$

Cross section passes for the checked types of loading.

4.5.2 Design check of the struts

The most loaded struts are the longer corner struts and therefore the design check is focused on them. The value of maximum normal force in these struts was taken from Scia Engineer and additional normal force from temperature was added to this value.

$N_{Ed,max,Scia} = 13\ 511.78\ kN$

$$N_{Ek,\Delta T} = \frac{A * E_s * \alpha * \Delta T}{1 + \frac{3 * n * A * E_s * H}{A_w * E_{soil} * L}} = \frac{7.8147 * 10^{-2} * 210 * 10^9 * 1.2 * 10^{-5} * 30}{1 + \frac{3 * 0.078147 * 210 * 10^9 * 20.85}{28.675 * 35 * 10^6 * 11.314}}$$

$$= 64.64\ kN$$

$N_{Ed,\Delta T} = N_{Ek,\Delta T} * \gamma_Q = 64.64 * 1.5 = 96.96\ kN$

$N_{Ed,max} = N_{Ed,max,Scia} + N_{Ed,\Delta T} = 13\ 511.78 + 96.96 = 13\ 608.74\ kN$

Design values of bending moments and shear forces are taken from Scia Engineer.

Maximum loads:

$N_{Ed,max} = 13\ 608.74\ kN\ (M_{eq} = M_{Ed,max})$

$V_{Ed,max} = 45.95\ kN$

$M_{Ed,max} = 129.96\ kNm$

According to EC 3 [11] the section of the strut is class 1.

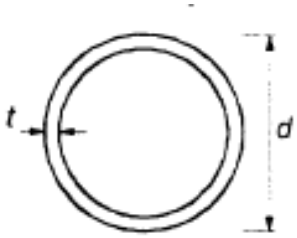

Figure 4.35 Cross sectional classification [11]

$$\frac{d}{t} = \frac{1020}{25} = 40.8 \leq 50\varepsilon^2 \quad ok$$

1. Compression ($N_{Ed,max} = 13\ 608.74\ kN$)

Bearing capacity:

$$N_{C,Rd} = \frac{A * f_y}{\gamma_{m0}} = \frac{7.8147 * 10^{-2} * 355 * 10^6}{1.0} = 27\ 742.19\ kN$$

Limit condition:

$$\frac{N_{Ed,max}}{N_{C,Rd}} = \frac{13\ 608.74}{27\ 742.19} = 0.49 \leq 1.0$$

2. Shear ($V_{Ed,max} = 45.95\ kN$)

Bearing capacity:

$$V_{pl,Rd} = \frac{A_v * (\frac{f_y}{\sqrt{3}})}{\gamma_{m0}} = \frac{0.0497 * (355 * \frac{10^6}{\sqrt{3}})}{1.0} = 10\ 186.48\ kN$$

Shearing area:

$$A_v = 2 * \frac{A}{\pi} = 2 * \frac{7.8147 * 10^{-2}}{\pi} = 0.0497\ m^2$$

Limit condition:

$$\frac{V_{max}}{V_{pl,Rd}} = \frac{45.95}{10\ 186.48} = 0.005 \leq 1.0$$

Because the ratio of V_{max} and $V_{pl,Rd}$ is smaller than 0.5 it is not necessary to reduce the yield stress for calculation of interaction of compression and bending.

3. Bending ($M_{Ed,y,max}$= *129.96 kNm*)

Bearing capacity:

$$M_{pl,Rd,y} = \frac{W_{pl,y} * f_y}{\gamma_{m0}} = \frac{2.4756 * 10^{-2} * 355 * 10^6}{1.0} = 8\ 788.38\ kNm$$

Limit condition:

$$\frac{M_{Ed,y,max}}{M_{pl,Rd,y}} = \frac{129.96}{8\ 788.38} = 0.015\ \leq 1.0$$

4. Buckling

Buckling capacity:

$$N_{b.Rd} = \frac{\chi * A * f_y}{\gamma_{m1}} = \frac{0.98 * 7.8147 * 10^{-2} * 355 * 10^6}{1.0} = 27\ 187.34\ kN$$

Buckling coefficient:

$$\chi = \frac{1}{\emptyset + \sqrt{\emptyset^2 - \lambda^2}} = \frac{1}{0.55 + \sqrt{0.55^2 - 0.29^2}} = 0.98 \leq 1.0$$

$$\emptyset = 0.5 * [1 + \alpha * (\lambda - 0.2) + \lambda^2] = 0.5 * [1 + 0.21 * (0.29 - 0.2) + 0.29^2] = 0.55$$

where α is coefficient of imperfection (buckling curve "a" → $\alpha = 0.21$)

Relative slenderness:

$$\lambda = \sqrt{\frac{A * f_y}{N_{cr}}} = \sqrt{\frac{7.8147 * 10^{-2} * 355 * 10^6}{0.32 * 10^9}} = 0.29$$

Critical force:

$$N_{cr} = \pi^2 * \frac{E * \mathrm{I}}{{L_{cr}}^2} = \pi^2 * \frac{210 * 10^9 * 9.6771 * 10^{-3}}{7.92^2} = 0.32 * 10^9\ N$$

Critical length:

$$L_{cr} = 0.7 * L = 0.7 * 11.314 = 7.92\ m$$

Limit condition:

$$\frac{N_{Ed,max}}{N_{b,Rd}} = \frac{13\ 608.74}{27\ 187.34} = 0.50 \leq 1.0 \qquad ok$$

5. Bending + Buckling

Interaction taken for $N_{Ed,max}$=*13 608.74 kN* and $M_{ed,y,max}$=*129.96 kNm*.

Limit condition:

$$\frac{N_{Ed}}{\frac{\chi_y * N_{Rk}}{\gamma_{m1}}} + k_{yy} * \frac{M_{y,Ed} + \Delta M_{y,Ed}}{\frac{\chi_{LT} * M_{y,Rk}}{\gamma_{m1}}} + k_{yz} * \frac{M_{z,Ed} + \Delta M_{z,Ed}}{\frac{M_{z,Rk}}{\gamma_{m1}}} \leq 1.0$$

where:

$\Delta M_{y,Ed} = \Delta M_{z,Ed} = 0\ kNm$

$M_{z,Ed} = 0\ kNm\ (caused\ only\ by\ self\ weight, small\ value\ possible\ to\ neglect)$

$\chi_{LT} = 1.0$

$N_{Rk} = f_y * A = 355 * 10^6 * 7.8147 * 10^{-2} = 27\,742.18\ kN$

$M_{y,Rk} = f_y * W_{Pl,y} = 355 * 10^6 * 2.4756 * 10^{-2} = 8\,788.38\ kNm$

Values of k_{yy}, k_{yz}, k_{zy}, k_{zz} are taken according to Annex B of EC 3 [11] (simplified method).

$$k_{yy} = C_{my} * \left(1 + \left(\lambda_y - 0.2\right) * \frac{N_{Ed}}{\frac{\chi_y * N_{Rk}}{\gamma_{m1}}}\right)$$

$$= 0.9 * \left(1 + (0.29 - 0.2) * \frac{13\,608.74}{\frac{0.98 * 27\,742.18}{1.0}}\right) = 0.94$$

$$\leq C_{my} * \left(1 + 0.8 * \frac{N_{Ed}}{\frac{\chi_y * N_{Rk}}{\gamma_{m1}}}\right) = 1.26 \quad ok$$

$C_{my} = 0.9$

$k_{yz} = 0.6 * k_{zz} = 0.6 * 0.94 = 0.564$

$C_{mz} = 0.9$

$k_{zz} = k_{yy} = 0.94$

Limit condition:

$$\frac{13\,608.74}{\frac{0.98 * 27\,742.18}{1.0}} + 0.94 * \frac{129.96 + 0}{\frac{1.0 * 8\,788.38}{1.0}} + 0 = 0.51 \leq 1.0 \qquad ok$$

- **z axis**

Limit condition:

$$\frac{N_{Ed}}{\frac{\chi_z * N_{Rk}}{\gamma_{m1}}} + k_{zy} * \frac{M_{y,Ed} + \Delta M_{y,Ed}}{\frac{\chi_{LT} * M_{y,Rk}}{\gamma_{m1}}} + k_{zz} * \frac{M_{z,Ed} + \Delta M_{z,Ed}}{\frac{M_{z,Rk}}{\gamma_{m1}}} \leq 1.0$$

$k_{zy} = 0.6 * k_{yy} = 0.6 * 0.94 = 0.564$

Check of limit condition:

$$\frac{13\,608.74}{\frac{0.98 * 27\,742.18}{1.0}} + 0.564 * \frac{129.96 + 0}{\frac{1.0 * 8\,788.38}{1.0}} + 0 = 0.51 \leq 1.0 \qquad ok$$

Cross section passes for the checked types of loading.

4.6 Disproportionate collapse (accidental loss of strut)

The design check for the loss of structural element is done for characteristic values of inner forces. The longer corner struts are the most loaded ones therefore on of these struts is taken out of the Scia model while the loads stay the same. Additional stress is created in the shorter strut in the corner and the waler beam is most loaded in places of the connection of this strut. The most loaded parts will be subjected to the design check.

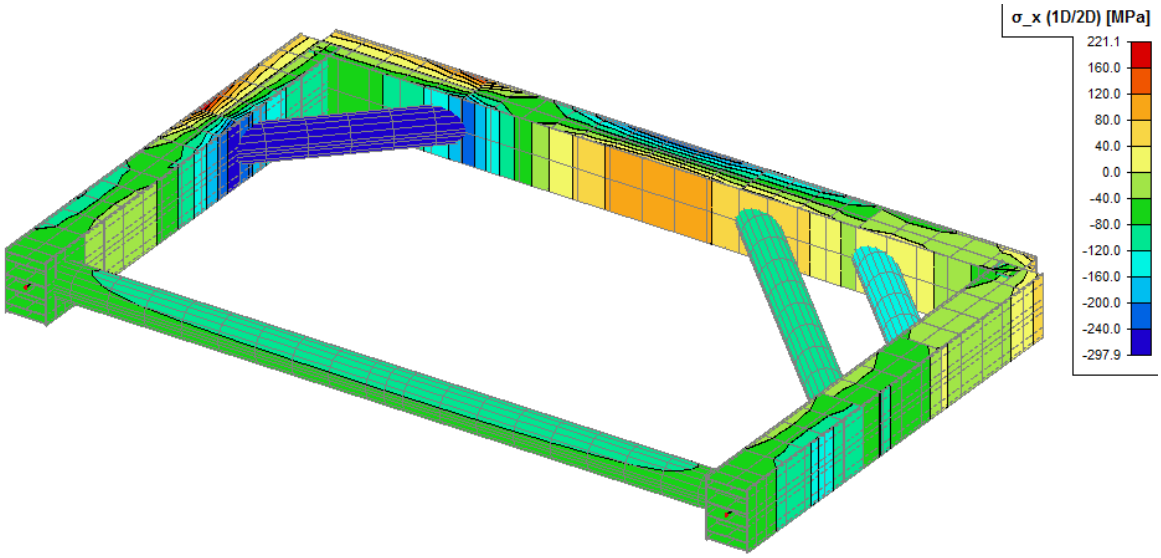

Figure 4.36 Stress in bracing frame after the loss of longer corner strut

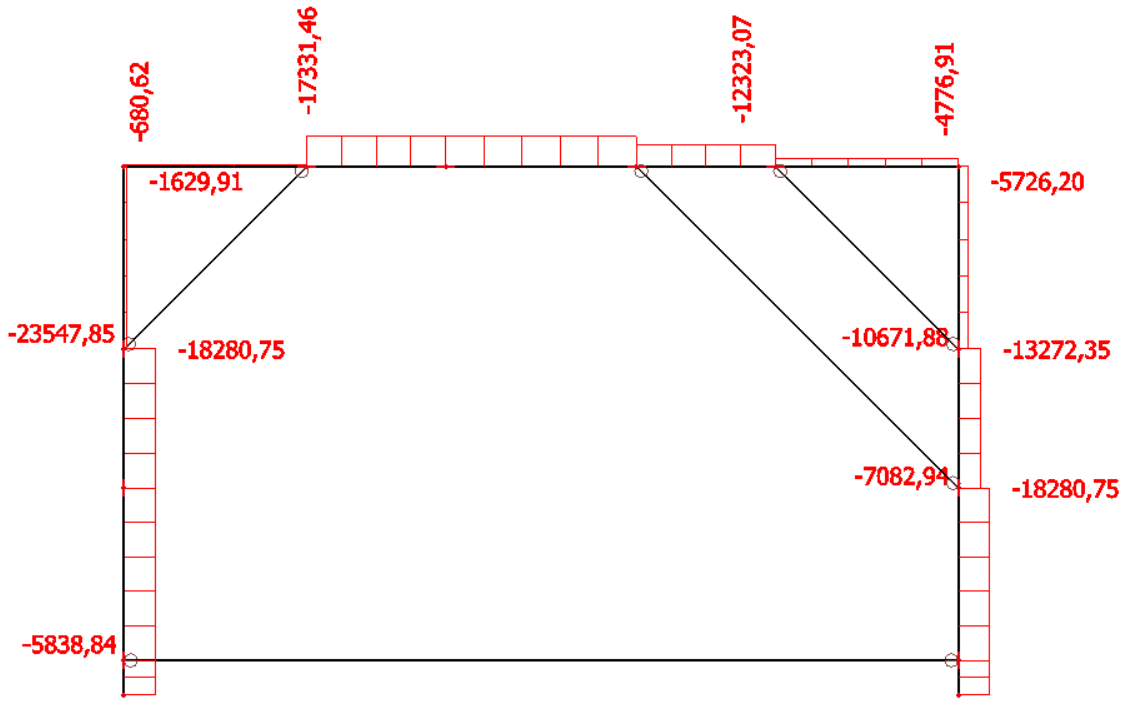

Figure 4.37 Normal forces N_{Ek} in frame

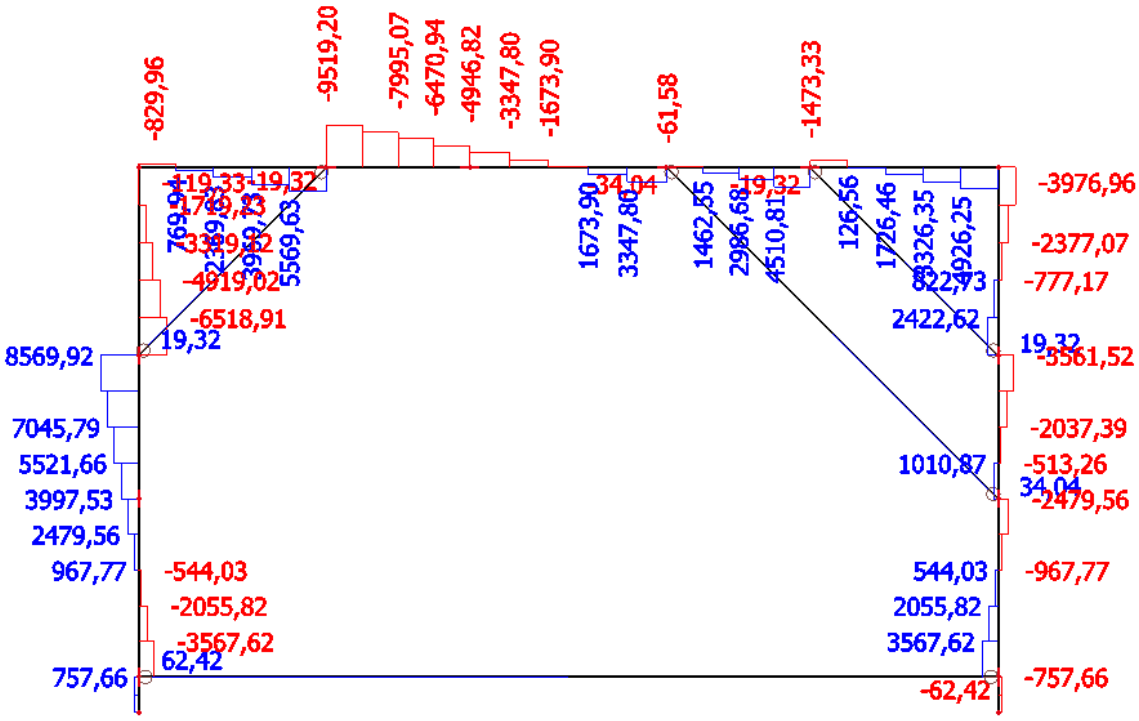

Figure 4.38 Shear forces V_{Ek} in frame

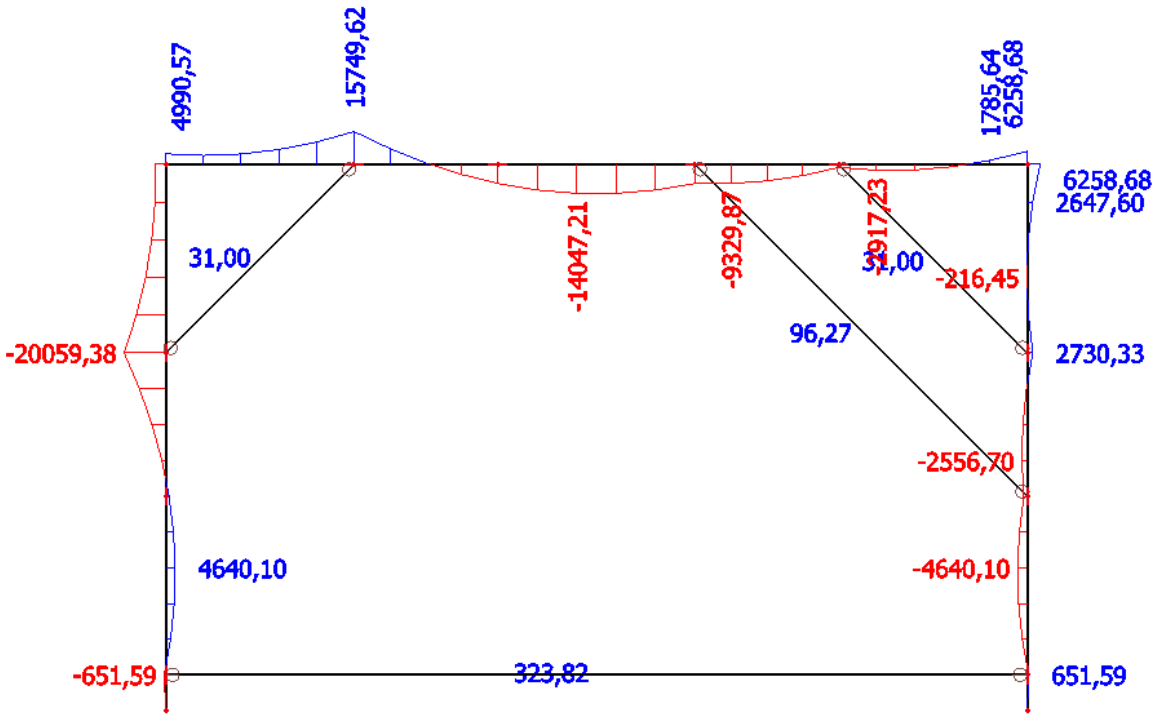

Figure 4.39 Bending moments M_{Ek} in frame

4.6.1 Waler beam design check

Bearing capacities:

$N_{pl,Rd} = 62\ 568.75\ kN\ (= N_{C,Rd})$

$V_{pl,Rd} = 23\ 879.20\ kN$

$M_{pl,Rd,y} = 24\ 855.95\ kNm$

Maximum loads:

$N_{Ed,max} = 18\ 280.75\ kN\ (M_{eq} = M_{Ed,max})$

$V_{Ed,max} = 9\ 519.20\ kN$

$M_{Ed,max} = 20\ 059.38\ kNm$

1. Compression ($N_{Ed,max} = 18\ 280.75\ kN$)

Limit condition:

$$\frac{N_{Ed,max}}{N_{C,Rd}} = \frac{18\ 280.75}{62\ 568.75} = 0.29 \leq 1.0$$

2. Shear ($V_{Ed,max}$ = *9 519.20 kN*)

Limit condition:

$$\frac{V_{Ed,max}}{V_{pl,Rd}} = \frac{9\ 519.20}{23\ 879.20} = 0.40\ \leq 1.0$$

Because the ratio of V_{max} and $V_{pl,Rd}$ is smaller than 0.5 therefore it is not necessary to reduce the yield stress.

3. Bending ($M_{Ed,y,max}$= *20 059.38 kNm*)

Limit condition:

$$\frac{M_{Ed,y,max}}{M_{pl,Rd,y}} = \frac{20\ 059.38}{24\ 855.95} = 0.81\ \leq 1.0$$

4. Buckling

- **y axis**

Buckling capacity:

$$N_{b.Rd,y} = \frac{\chi_y * A * f_y}{\gamma_{m1}} = \frac{1.0 * 0.2665 * 235 * 10^6}{1.0} = 62\ 568.75\ kN$$

Buckling coefficient:

$$\chi_y = \frac{1}{\emptyset_y + \sqrt{\emptyset_y{}^2 - \lambda_y{}^2}} = \frac{1}{0.497 + \sqrt{0.497^2 - 0.13^2}} = 1.02 \leq 1.0 \rightarrow\ \chi_y = 1.0$$

$$\emptyset_y = 0.5 * \left[1 + \alpha * \left(\lambda_y - 0.2\right) + \lambda_y{}^2\right] = 0.5 * [1 + 0.34 * (0.13 - 0.2) + 0.13^2]$$
$$= 0.497$$

where α is coefficient of imperfection (buckling curve "b" → $\alpha = 0.34$)

Relative slenderness:

$$\lambda_y = \sqrt{\frac{A * f_y}{N_{cr,y}}} = \sqrt{\frac{0.26625 * 235 * 10^6}{3.71 * 10^9}} = 0.13$$

Critical force:

$$N_{cr,y} = \pi^2 * \frac{E * I_y}{L_{cr}{}^2} = \pi^2 * \frac{210 * 10^9 * 5.2683 * 10^{-2}}{5.425^2} = 3.71 * 10^9\ N$$

Critical length:

$$L_{cr} = 0.7 * L = 0.7 * 7.75 = 5.425\ m$$

Limit condition:

$$\frac{N_{Ed,max}}{N_{b,Rd,y}} = \frac{18\ 280.75}{62\ 568.75} = 0.32 \leq 1.0 \qquad ok$$

- **z axis**

Buckling capacity:

$$N_{b.Rd,z} = \frac{\chi_z * A * f_y}{\gamma_{m1}} = \frac{1.0 * 0.26625 * 235 * 10^6}{1.0} = 62\ 568.75\ kN$$

Buckling coefficient:

$$\chi_z = \frac{1}{\emptyset_z + \sqrt{\emptyset_z{}^2 - \lambda_z{}^2}} = \frac{1}{0.488 + \sqrt{0.488^2 - 0.1^2}} = 1.04 \leq 1.0 \rightarrow \chi_z = 1.0$$

$$\emptyset_z = 0.5 * \left[1 + \alpha * (\lambda_z - 0.2) + \lambda_z{}^2\right] = 0.5 * [1 + 0.34 * (0.1 - 0.2) + 0.1^2] = 0.488$$

where α is coefficient of imperfection (buckling curve "b" → $\alpha = 0.34$)

Relative slenderness:

$$\lambda_z = \sqrt{\frac{A * f_y}{N_{cr,z}}} = \sqrt{\frac{0.26625 * 235 * 10^6}{6.31 * 10^9}} = 0.10$$

Critical force:

$$N_{cr,z} = \pi^2 * \frac{E * I_z}{L_{cr}{}^2} = \pi^2 * \frac{210 * 10^9 * 8.9623 * 10^{-2}}{5.425^2} = 6.31 * 10^9\ N$$

Limit condition:

$$\frac{N_{Ed,max}}{N_{b,Rd,z}} = \frac{18\ 280.75}{62\ 568.75} = 0.32 \leq 1.0 \qquad ok$$

5. <u>Bending + Buckling</u>

- **y axis**

$$\frac{N_{Ed}}{\frac{\chi_y * N_{Rk}}{\gamma_{m1}}} + k_{yy} * \frac{M_{y,Ed} + \Delta M_{y,Ed}}{\frac{\chi_{LT} * M_{y,Rk}}{\gamma_{m1}}} + k_{yz} * \frac{M_{z,Ed} + \Delta M_{z,Ed}}{\frac{M_{z,Rk}}{\gamma_{m1}}} \leq 1.0$$

where:

$\Delta M_{y,Ed} = \Delta M_{z,Ed} = 0\ kNm$

$M_{z,Ed} = 0\ kNm\ (caused\ only\ by\ self\ weight, small\ value\ possible\ to\ neglect)$

$\chi_{LT} = 1.0$

$N_{Rk} = f_y * A = 235 * 10^6 * 0.26625 = 62\ 568.75\ kN$

$$M_{y,Rk} = f_y * W_{Pl,y} = 235 * 10^6 * 0.10577 = 24\,855.95\ kNm$$
$$M_{z,Rk} = f_y * W_{Pl,z} = 235 * 10^6 * 0.1367 = 32\,124.5\ kNm$$

Values of k_{yy}, k_{yz}, k_{zy}, k_{zz} are taken according to Annex B of EC 3 [11] (simplified method).

$$k_{yy} = C_{my} * \left(1 + \left(\lambda_y - 0.2\right) * \frac{N_{Ed}}{\frac{\chi_y * N_{Rk}}{\gamma_{m1}}}\right)$$
$$= 0.9 * \left(1 + (0.13 - 0.2) * \frac{18\,280.75}{\frac{1.0 * 62\,568.75}{1.0}}\right) = 0.88$$
$$\leq C_{my} * \left(1 + 0.8 * \frac{N_{Ed}}{\frac{\chi_y * N_{Rk}}{\gamma_{m1}}}\right) = 1.11 \quad ok$$

$C_{my} = 0.9$

$C_{mz} = 0.9$

Limit condition:

$$\frac{18\,280.75}{\frac{1.0 * 62\,568.75}{1.0}} + 0.88 * \frac{20\,059.38 + 0}{\frac{1.0 * 24\,855.95}{1.0}} + 0 = 1.0 \leq 1.0 \qquad ok$$

- **z axis**

$$\frac{N_{Ed}}{\frac{\chi_z * N_{Rk}}{\gamma_{m1}}} + k_{zy} * \frac{M_{y,Ed} + \Delta M_{y,Ed}}{\frac{\chi_{LT} * M_{y,Rk}}{\gamma_{m1}}} + k_{zz} * \frac{M_{z,Ed} + \Delta M_{z,Ed}}{\frac{M_{z,Rk}}{\gamma_{m1}}} \leq 1.0$$

$$k_{zz} = C_{mz} * \left(1 + (\lambda_z - 0.2) * \frac{N_{Ed}}{\frac{\chi_z * N_{Rk}}{\gamma_{m1}}}\right) = 0.9 * \left(1 + (0.1 - 0.2) * \frac{18\,280.25}{\frac{1.0 * 62\,568.75}{1.0}}\right)$$
$$= 0.87 \leq C_{mz} * \left(1 + 0.8 * \frac{N_{Ed}}{\frac{\chi_z * N_{Rk}}{\gamma_{m1}}}\right) = 1.11 \quad ok$$

$k_{zy} = 0.6 * k_{yy} = 0.6 * 0.88 = 0.53$

Limit condition:

$$\frac{18\ 280.25}{\frac{1.0 * 62\ 568.75}{1.0}} + 0.53 * \frac{20\ 059.38 + 0}{\frac{1.0 * 24\ 855.95}{1.0}} + 0 = 0.72 \leq 1.0 \qquad ok$$

Cross section passes for the checked types of loading.

4.6.2 Strut design check

The most loaded strut is now the shorter corner. The effect of temperature is not considered for this part of design check and all values of inner forces are taken directly from Scia engineer model.

Bearing capacities:

$N_{pl,Rd} = 27\ 742.19\ kN\ (= N_{C,Rd})$

$V_{pl,Rd} = 10\ 186.48\ kN$

$M_{pl,Rd,y} = 8\ 788.38\ kNm$

Maximum loads:

$N_{Ed,max} = 23\ 547.85\ kN$

$V_{Ed,max} = 19.32\ kN$

$M_{Ed,z,max} = 31.0\ kNm$

1. Compression ($N_{Ed,max} = 23\ 547.85\ kN$)

Limit condition:

$$\frac{N_{Ed,max}}{N_{C,Rd}} = \frac{13\ 608.74}{27\ 742.19} = 0.49 \leq 1.0$$

2. Shear

Not necessary to check because of small values of inner forces.

3. Bending

Not necessary to check because of small values of inner forces.

4. Buckling

Buckling capacity:

$$N_{b.Rd} = \frac{\chi * A * f_y}{\gamma_{m1}} = \frac{1.0 * 7.8147 * 10^{-2} * 355 * 10^6}{1.0} = 27\ 742.19\ kN$$

Buckling coefficient:

$$\chi = \frac{1}{\emptyset + \sqrt{\emptyset^2 - \lambda^2}} = \frac{1}{0.51 + \sqrt{0.51^2 - 0.167^2}} = 1.0 \leq 1.0$$

$$\emptyset = 0.5 * [1 + \alpha * (\lambda - 0.2) + \lambda^2] = 0.5 * [1 + 0.21 * (0.167 - 0.2) + 0.167^2] = 0.51$$

where α is coefficient of imperfection (buckling curve "a" → $\alpha = 0.21$)

Relative slenderness:

$$\lambda = \sqrt{\frac{A * f_y}{N_{cr}}} = \sqrt{\frac{7.8147 * 10^{-2} * 355 * 10^6}{0.99 * 10^9}} = 0.167$$

Critical force:

$$N_{cr} = \pi^2 * \frac{E * \mathrm{I}}{{L_{cr}}^2} = \pi^2 * \frac{210 * 10^9 * 9.6771 * 10^{-3}}{4.49^2} = 0.99 * 10^9\ N$$

Critical length:

$$L_{cr} = 0.7 * L = 0.7 * 6.421 = 4.49\ m$$

Limit condition:

$$\frac{N_{Ed,max}}{N_{b,Rd}} = \frac{23\ 547.85}{27\ 742.19} = 0.85 \leq 1.0 \qquad ok$$

5. Bending + Buckling

Interaction taken for $N_{Ed,max}$=*23 547.85 kN* and $M_{ed,y,max}$=*31.0 kNm*.

Limit condition:

$$\frac{N_{Ed}}{\frac{\chi_y * N_{Rk}}{\gamma_{m1}}} + k_{yy} * \frac{M_{y,Ed} + \Delta M_{y,Ed}}{\frac{\chi_{LT} * M_{y,Rk}}{\gamma_{m1}}} + k_{yz} * \frac{M_{z,Ed} + \Delta M_{z,Ed}}{\frac{M_{z,Rk}}{\gamma_{m1}}} \leq 1.0$$

where:

$\Delta M_{y,Ed} = \Delta M_{z,Ed} = 0\ kNm$

$M_{z,Ed} = 0\ kNm\ (caused\ only\ by\ self\ weight, small\ value\ possible\ to\ neglect)$

$\chi_{LT} = 1.0$

$N_{Rk} = f_y * A = 355 * 10^6 * 7.8147 * 10^{-2} = 27\ 742.18\ kN$

$M_{y,Rk} = f_y * W_{Pl,y} = 355 * 10^6 * 2.4756 * 10^{-2} = 8\ 788.38\ kNm$

Values of k_{yy}, k_{yz}, k_{zy}, k_{zz} are taken according to Annex B of EC 3 [11] (simplified method).

$$k_{yy} = C_{my} * \left(1 + \left(\lambda_y - 0.2\right) * \frac{N_{Ed}}{\frac{\chi_y * N_{Rk}}{\gamma_{m1}}} \right)$$

$$= 0.9 * \left(1 + (0.167 - 0.2) * \frac{23\,547.85}{\frac{1.0 * 27\,742.18}{1.0}} \right) = 0.87$$

$$\leq C_{my} * \left(1 + 0.8 * \frac{N_{Ed}}{\frac{\chi_y * N_{Rk}}{\gamma_{m1}}} \right) = 1.51 \quad ok$$

$C_{my} = 0.9$

$k_{yz} = 0.6 * k_{zz} = 0.6 * 0.87 = 0.52$

$C_{mz} = 0.9$

$k_{zz} = k_{yy} = 0.87$

Limit condition:

$$\frac{23\,547.85}{\frac{1.0 * 27\,742.18}{1.0}} + 0.87 * \frac{31.0 + 0}{\frac{1.0 * 8\,788.38}{1.0}} + 0 = 0.85 \leq 1.0 \qquad ok$$

- **z axis**

$k_{zy} = 0.6 * k_{yy} = 0.6 * 0.87 = 0.564$

Limit condition:

$$\frac{23\,547.85}{\frac{1.0 * 27\,742.18}{1.0}} + 0.564 * \frac{31.0 + 0}{\frac{1.0 * 8\,788.38}{1.0}} + 0 = 0.85 \leq 1.0 \qquad ok$$

Cross section passes for the checked types of loading.

Summary

At the beginning of the thesis there is a brief description of the virtual project of a shaft where one of the diaphragm walls is affected by excavation from both sides. Additionally, the first chapter deals with construction sequence in detail. There is a given course of construction of diaphragm walls for this project. Furthermore, the excavation phases for both the shaft and metro station are described. At the end metro tubes are constructed and the shaft is backfilled.

In the second chapter there is an assessment of geological survey and geological conditions. Geotechnical parameters for all soil and rock stratum are stated in this chapter. Also the groundwater is mentioned there.

Third chapter deals with thermal loads on struts. This chapter was carried out as a research from available literature. The results of the research were used later in the thesis for calculation of the additional normal force in strut caused by temperature changes.

Fourth chapter is composed of two main parts – one part deals with analytical models and another part deals with design checks of diaphragm wall and lateral support frame. Three different programs were used for development of the analytical models. At first the models in software Plaxis were carried out. One of the models uses Modified Cam Clay material model with undrained conditions for Clay strata, another two use Mohr-Coulomb material model (one with undrained and one with drained conditions) for Clay strata. Then a model with subgrade reaction was undertaken in Geo 5. The outputs of these models were compared in this chapter. The last model was in Scia Engineer and it only regards the lateral support frame. Outputs of CC model in Plaxis and of Scia Engineer were used for design checks. There are 8 types of reinforcement schemes changing according to the bending moments' envelope in design values. Reinforcement bars of diameters 25 and 40 mm were used for the structure. The bars are placed in one, two, three and four layers. Considering the lateral support frame the values of inner forces were taken from Scia Engineer and an additional normal force from changes in temperature was added to these values. Design check was done for the fourth level of bracing that is the most loaded one. Waler beam was considered to be from steel grade S235 and struts from steel grade S355. Diaphragm wall and lateral support frame are satisfactory for the loads given in this thesis.

List of references

1. **P.Makásek, P.Havlan, B.Polák.** METRO V BAKU: FIALOVÁ LINKA – STARTOVACÍ ŠACHTA LS04. *Tunel.* 2015, Sv. č.1.
2. *http://technologie.fsv.cvut.cz/aitom/podklady/online-zakladani/textjama322.html.* [Online]
3. **Zakládání staveb.** http://www.zakladani.cz/. [Online]
4. *http://www.bacsol.co.uk/technique/diaphragm-walls/.* [Online]
5. *http://www.deepexcavation.com/en/Diaphragm+wall+construction+methods.* [Online]
6. **Mott MacDonald.**
7. **Gould, Tony.** www.vpgroundforce.com/gb/media-hub/articles/groundforce-blog/. [Online]
8. *Performance of a braced excavation in granular and cohesive soils.* **K.R.Chapman, E.J. Cording, H. Schnabel.** 1972.
9. *EN 1992-1-1.*
10. *EN 1997 - Design approach 2.*
11. *EN 1993-1.*
12. *EN 206-1 Concrete - Part 1: Specification, performance, production and conformity.*

List of short cuts and symbols

A	cross-sectional area
$A_s = A_{sprov}$	cross sectional area of reinforcement
$A_{s,max}$	maximum cross sectional area of reinforcement
$A_{s,min}$	minimum cross sectional area of reinforcement
$A_{s,rqd}$	minimum required cross sectional area of reinforcement
$A_{s,v,max}$	maximum cross sectional area of reinforcement for walls
$A_{s,v,min}$	minimum cross sectional area of reinforcement for walls
A_{strut}	cross-sectional area of strut
A_v	shear area
b	overall width of a cross-section
C_c	compression index
C_s	recompression index
c	concrete cover
c´	effective ground cohesion
c'_{ref}	effective ground cohesion for interface
D-wall	diaphragm wall
d	diameter
d	effective depth of a cross-section
d	width of an element
d_g	largest nominal maximum aggregate size
E	modulus of elasticity
E_{oed}	oedometric deformation modulus
E´	effective modulus of elasticity
E_s	elastic modulus of steel
E_{cm}	secant modulus of elasticity of concrete
EA	axial stiffness
EI	bending stiffness
EPB	earth pressure balance
e_{init}	initial void ratio
FEM	finite element method
f_{ck}	characteristic compressive cylinder strength of concrete at 28 days
f_{cd}	design value of concrete compressive strength

f_y	yield strength of steel
f_{yk}	characteristic yield strength of reinforcement
f_{yd}	design yield strength of reinforcement
G	modulus of elasticity in shear
h	overall depth of a cross-section
h_w	web height
I	moment of inertia
K_0	at-rest earth pressures coefficient
k_{ij}	interaction factors
k_h	modulus of subgrade reaction
L_{cr}	critical length
LE	linear elasticity
M_{ed}	design value of the applied bending moment
M_{ek}	characteristic value of the applied bending moment
$M_{c,Rd}$	design bearing capacity in bending
M_{Rd}	bearing capacity of bending moment
MC	Mohr-Coulomb
$N_{b,Rd}$	buckling bearing capacity
N_{cr}	critical force
$N_{c,Rd}$	design bearing capacity in axial compression
N_{ed}	design value of the applied axial force (tension or compression)
N_{ek}	characteristic value of the applied axial force (tension or compression)
N_{Rd}	bearing capacity of normal force
R_{inter}	interface parameter
S_u	undrained shear strength
s_{max}	maximum spacing of reinforcement bars
s_{min}	minimal spacing of reinforcement bars
s_s	spacing of stirrups
SPB	slurry pressure balance
TBM	tunnel boring machine
t	thickness
t_w	web thickness
ULS	ultimate limit state
u_x	horizontal displacement

u_y	vertical displacement
V_{ed}	design value of the applied shear force
$V_{pl,Rd}$	plastic shear bearing capacity
W	section modulus
w	self -weight
x	neutral axis depth
z	lever arm of internal forces
α	coefficient of thermal expansion
α	coefficient of imperfections
α_{cc}	coefficient taking account of long term effects on the compressive strength and of unfavourable effects resulting from the way the load is applied
γ	unit weight of soil
γ_c	partial factor for concrete
γ_G	partial factor for permanent actions
γ_m	material resistance factor
γ_s	partial factor for reinforcing steel
γ_{steel}	unit weight of structural steel
ε_{cu3}	ultimate compressive strain in the concrete
ε_{yk}	strain in reinforcing steel
η	factor defining the effective strength
λ	factor defining the effective height of the compression zone
λ	relative slenderness
λ	Cam Clay compression index
ϕ	diameter of a reinforcing bar
ϕ_s	diameter of a stirrup
φ'	effective angle of internal friction
φ_{cv}	critical state friction angle
ν	Poisons ratio
ν'_{ur}	Poisson's ratio for unloading-reloading
κ	Cam Clay swelling index
χ	buckling coefficient (for axial compression)
χ_{LT}	buckling coefficient

List of Appendices